

UC Riverside

UC Riverside Previously Published Works

Title

Artificial Greenhouse Gases as Exoplanet Technosignatures

Permalink

<https://escholarship.org/uc/item/3zp8b7qc>

Journal

The Astrophysical Journal, 969(1)

ISSN

0004-637X

Authors

Schwieterman, Edward W

Faucher, Thomas J

Haqq-Misra, Jacob

et al.

Publication Date

2024-07-01

DOI

10.3847/1538-4357/ad4ce8










Copyright Information

This work is made available under the terms of a Creative Commons Attribution License, available at <https://creativecommons.org/licenses/by/4.0/>

Peer reviewed



Artificial Greenhouse Gases as Exoplanet Technosignatures

Edward W. Schwieterman^{1,2} , Thomas J. Fauchez^{3,4,5} , Jacob Haqq-Misra² , Ravi K. Kopparapu^{3,4} ,
Daniel Angerhausen^{2,6,7} , Daria Pidhorodetska¹ , Michaela Leung¹ , Evan L. Sneed¹ , and Elsa Ducrot^{8,9} 

¹Department of Earth and Planetary Sciences, University of California, Riverside, CA, USA; eschwiet@ucr.edu

²Blue Marble Space Institute of Science, Seattle, WA, USA

³NASA Goddard Space Flight Center, 8800 Greenbelt Road, Greenbelt, MD 20771, USA

⁴Sellers Exoplanet Environment Collaboration (SEEC), NASA Goddard Space Flight Center, USA

⁵Integrated Space Science and Technology Institute, Department of Physics, American University, Washington DC, USA

⁶ETH Zurich, Institute for Particle Physics & Astrophysics, Wolfgang-Pauli-Str. 27, 8093 Zurich, Switzerland

⁷National Center of Competence in Research PlanetS, Gesellschaftsstrasse 6, 3012 Bern, Switzerland

⁸LESIA, Observatoire de Paris, CNRS, Université Paris Diderot, Université Pierre et Marie Curie, 5 place Jules Janssen, 92190 Meudon, France

⁹AIM, CEA, CNRS, Université Paris-Saclay, Université de Paris, F-91191 Gif-sur-Yvette, France

Received 2024 January 4; revised 2024 April 24; accepted 2024 May 15; published 2024 June 25

Abstract

Atmospheric pollutants such as chlorofluorocarbons and NO₂ have been proposed as potential remotely detectable atmospheric technosignature gases. Here we investigate the potential for artificial greenhouse gases including CF₄, C₂F₆, C₃F₈, SF₆, and NF₃ to generate detectable atmospheric signatures. In contrast to passive incidental by-products of industrial processes, artificial greenhouse gases would represent an intentional effort to change the climate of a planet with long-lived, low-toxicity gases and would possess low false positive potential. An extraterrestrial civilization may be motivated to undertake such an effort to arrest a predicted snowball state on their home world or to terraform an otherwise uninhabitable terrestrial planet within their system. Because artificial greenhouse gases strongly absorb in the thermal mid-infrared window of temperate atmospheres, a terraformed planet will logically possess strong absorption features from these gases at mid-infrared wavelengths (~8–12 μm), possibly accompanied by diagnostic features in the near-infrared. As a proof of concept, we calculate the needed observation time to detect 1 [10](100) ppm of C₂F₆/C₃F₈/SF₆ on TRAPPIST-1 f with JWST MIRI's Low Resolution Spectrometer (LRS) and NIRSpec. We find that a combination of 1[10](100) ppm each of C₂F₆, C₃F₈, and SF₆ can be detected with a signal-to-noise ratio ≥ 5 in as few as 25[10](5) transits with MIRI/LRS. We further explore mid-infrared direct-imaging scenarios with the Large Interferometer for Exoplanets mission concept and find these gases are more detectable than standard biosignatures at these concentrations. Consequently, artificial greenhouse gases can be readily detected (or excluded) during normal planetary characterization observations with no additional overhead.

Unified Astronomy Thesaurus concepts: [Technosignatures \(2128\)](#); [Exoplanet atmospheres \(487\)](#); [Exoplanets \(498\)](#); [Astrobiology \(74\)](#); [Habitable planets \(695\)](#); [Biosignatures \(2018\)](#); [Greenhouse gases \(684\)](#); [Search for extraterrestrial intelligence \(2127\)](#)

1. Introduction

Detecting life beyond Earth is one of the foundational goals of astrobiology. The specific search for remote indicators of life on exoplanets is a major driver for the design of near to intermediate future space-based mission concepts (National Academies of Sciences, Engineering, & Medicine & others 2019, 2018, 2023; LUVUOIR-Team 2019; Gaudi et al. 2020). Biosignatures are spectroscopic or temporal indications that a planet is inhabited with simple (nontechnological) life. Common examples of biosignatures include O₂, O₃, CH₄, N₂O, and the vegetation red-edge (Seager et al. 2012; Kaltenecker 2017; Schwieterman et al. 2018), although biosignature interpretations are strongly dependent on planetary context in order to avoid the potential for false positives (e.g., Meadows et al. 2018). In contrast, technosignatures are observational indications of technology that can be detected via astronomical means, which may encompass technological civilizations or the technology left behind by biological or

artificial intelligence (Tarter 2007; Haqq-Misra et al. 2022b). Technosignatures may include radio transmissions (Cocconi & Morrison 1959; Tarter 2001; Worden et al. 2017), laser pulses (Stone et al. 2005; Howard et al. 2007; Vides et al. 2019), megastructures (Dyson 1960; Shkadov 1988; Wright 2020), or modifications to the surface or atmosphere of an inhabited (or noninhabited) planet such as solar panels (Lingam & Loeb 2017), city lights (Beatty 2022), or artificial atmospheric gases (Lin et al. 2014; Haqq-Misra et al. 2022a; Seager et al. 2023). See Haqq-Misra et al. (2022b) for a recent review of the search for technosignatures with current and future missions.

Because of the immense distances involved, the search for exoplanetary life is necessarily a search for global biospheres where native life has left a substantial impact on the atmosphere or surface of the planet. The science of exoplanet biosignatures has thus developed to assess candidate planetary biosignatures based on their intrinsic detectability (i.e., absorption properties), ability to accumulate to high concentrations in the atmosphere (i.e., robustness to photochemical reactions that destroy them), and their separability from abiotic planetary processes that would confound interpretations of biogenicity (e.g., Meadows et al. 2018; Schwieterman et al. 2018). The near future potential for characterizing terrestrial



Original content from this work may be used under the terms of the [Creative Commons Attribution 4.0 licence](#). Any further distribution of this work must maintain attribution to the author(s) and the title of the work, journal citation and DOI.

exoplanetary atmospheres and surfaces in search of remote biosignatures has opened up the possibility for commensal searches for planetary technosignatures with no added cost (Lingam & Loeb 2019). Commensal search programs are already common within SETI, especially when conducting radio-based observations, e.g., SERENDIP (Bowyer et al. 1988; Sullivan et al. 1997), Allen Telescope Array (DeBoer 2006), MeerKAT (Czech et al. 2021), and COSMIC (Tremblay et al. 2024). In a similar vein to the search for biosignatures, planetary technosignatures (technosignatures limited to the planetary scale, excluding, e.g., stellar megastructures) are functionally a search for “technospheres,” where the impact of technology has detectably risen above the nontechnological (abiotic and biotic) background level of the planetary environment (Frank et al. 2017; Haqq-Misra et al. 2020).

In contrast to biosignatures, many technosignatures may provide greater specificity (less “false positive” potential), as many putative technosignatures have more limited abiotic formation channels when compared to biosignatures. On the other hand, technosignatures may be short-lived when compared to biosignatures (Sheikh 2020). If we only take our planet as an example, atmospheric biosignatures may have persisted for up to 4 Gyr (Krissansen-Totton et al. 2018b; Olson et al. 2018), while our civilizational technosignatures are, at most, centuries old. Potential atmospheric technosignatures are further limited by practical observational considerations if such targets are restricted to the same systems where biosignature searches are to be conducted. In a volume-limited survey that includes only the nearest systems where angular resolution constraints allow habitable zones to be directly imaged—for example the ~ 25 systems recommended by the National Academy of Sciences 2020 Astronomy and Astrophysics Decadal Survey for the next-generation IR/optical/UV surveyor telescope (National Academies of Sciences, Engineering, & Medicine & others 2023)—it would seem vanishingly unlikely to detect atmospheric technosignatures if we take at face value the ratio of the longevity of technosignatures to biosignatures on Earth. However, Wright et al. (2022) argue that this view is based on the untested premise that nontechnological biospheres are more common than technospheres. In contrast to the constraints of simple life, technological life is not necessarily limited to one planetary or stellar system, and moreover, certain technologies could persist over astronomically significant periods of time. We know neither the upper limit nor the average timescale for the longevity of technological societies (not to mention abandoned or automated technology), given our limited perspective of human history. An observational test is therefore necessary before we outright dismiss the possibility that technospheres are sufficiently common to be detectable in the nearby Universe (Haqq-Misra et al. 2020).

Atmospheric pollutants such as chlorofluorocarbons (CFCs) and NO_2 have been proposed as potential remotely detectable atmospheric technosignature gases (Lin et al. 2014; Koppappu et al. 2021; Haqq-Misra et al. 2022a). However, these compounds are incidental products of industrial civilization and have several deleterious impacts on the planetary environment and on the civilization producing them. For example, CFCs promote the destruction of the ozone layer (Solomon 1999) and NO_2 causes respiratory toxicity (Elsayed 1994). Recent years have seen the dramatic reduction of CFC (and related hydrofluorocarbons) use on Earth due to the

Montreal Protocol and subsequent amendments (Hu et al. 2017; Fahey et al. 2018). Because industrial NO_2 is most often produced as a result of combustion, its production would fall precipitously if fossil fuels were to be phased out. It is therefore possible, even likely, that the window to observe these pollutant gases on a planet inhabited by an industrial civilization would be short in geologic terms.

We propose that certain atmospheric technosignatures do not suffer from this longevity problem. In contrast to industrial pollutants, artificial greenhouse (“terraforming”) gases would represent an intentional effort to modify a planet’s climate, and could persist for the entire remaining history of a civilization or beyond. Terraforming, by definition, requires sufficient modification of the atmosphere to adjust a planet’s global energy balance, which correspondingly implies a large spectral signature in the thermal infrared portion of the planet’s spectrum, incidentally supporting remote detectability. Maintaining a terraformed atmosphere may also require the consistent and intentional replenishment of the contributing gases. Fortuitously, many such gases tend to have long atmospheric residence times of thousands to tens of thousands of years (e.g., Mühle et al. 2010), which would help make the cost of doing so nonprohibitive. Civilizations may be motivated to introduce highly efficient greenhouse gases to forestall a global ice age on their own home world caused by analogs to Earth’s Milankovich cycles (Berger 1988; Haqq-Misra 2014). Alternatively, they may use terraforming gases to make another planet in their home system (or beyond) more suitable for life, as humans have proposed for Mars (e.g., Graham 2004; Marinova et al. 2005; Dicaire et al. 2013; Pařka et al. 2022). For the case of Mars, the idea of mobilizing available CO_2 and other volatile inventories as a terraforming strategy appears to be largely infeasible (Jakosky & Edwards 2018), so the use of additional artificial gases would be needed for an effective terraforming strategy.

A handful of previous studies have studied the use of artificial greenhouse gases for terraforming. Marinova et al. (2005) examine the potential efficacy of several artificial greenhouse gases including carbon tetrafluoride (CF_4), hexafluoroethane (C_2F_6), perfluoropropane (C_3F_8), and sulfur hexafluoride (SF_6) to warm modern Mars. These fluorine-bearing gases were chosen in part because of their nontoxic nature and their relative inertness compared to chlorine- or bromine-containing greenhouse gases that catalytically destroy ozone. On a per-molecule basis, each of these species is a far more effective greenhouse gas than CO_2 or H_2O due to strong and broad absorption features that overlap with the mid-infrared (MIR) window of a habitable exoplanet ($\sim 8\text{--}12\ \mu\text{m}$; Mühle et al. 2010; Totterdill et al. 2016; Kovács et al. 2017). Marinova et al. (2005) found that C_3F_8 has the largest warming potential of any single gas, but that a mixture of these four gases would be more effective than any one gas alone due to their nonoverlapping absorption features. Dicaire et al. (2013) similarly examined the warming potential of CF_4 , C_2F_6 , C_3F_8 , and SF_6 using a Martian global climate model.

Haqq-Misra et al. (2022b) suggested that future exoplanet characterization missions should search for these artificial greenhouse gases including perfluorocarbons (PFCs; C_xF_y), SF_6 , and nitrogen trifluoride (NF_3 ; see their Figures 1 and 3). Elowitz (2022) noted that artificial greenhouse gases such as CFCs, PFCs, and other fluorinated gases including NF_3 and SF_6 , would be ideal technosignature candidates. Seager et al. (2023)

argue that the fully fluorinated gases SF_6 and NF_3 are particularly compelling technosignatures because they are unlikely to be produced biologically, are produced at low-abiotic rates, and possess spectral features that do not overlap significantly with common gases. While the detectability of CFCs with JWST has been studied (Lin et al. 2014; Haqq-Misra et al. 2022a), to our knowledge, no existing study has quantitatively examined the detectability of PFCs or other fully fluorinated gases with JWST or future observatories, particularly in the context of terraformed planets.

Here we examine the potential detectability of C_2F_6 , C_3F_8 , SF_6 , NF_3 , and CF_4 with current and future observatories using a combination of radiative transfer and instrument simulation models as a first-pass “proof of concept” for detecting artificial greenhouse gases and terraformed planets. We produce both synthetic transmission spectra applicable to observations and emission (thermal infrared) spectra. We correspondingly conduct detectability analyses for a TRAPPIST-1 f-like exoplanet (chosen because it is in the outer habitable zone) with JWST and directly imaged terraformed terrestrial outer habitable zone planets with the Large Interferometer for Exoplanets (LIFE) mission concept (Quanz et al. 2022). While we do not conduct self-consistent climate calculations, we do examine the detectability of these gases individually and in combination at levels of 1, 10, and 100 ppm in a 1 bar Earth-like atmosphere, consistent with the range explored by Marinova et al. (2005) that would result in appreciable greenhouse warming on a Mars-like planet ($\sim 1\text{--}40$ K). We apply our results to inform a generalized approach for fingerprinting exoplanetary atmospheres with artificial greenhouse warming, which should produce an anomalous MIR signature possibly accompanied by incidental but diagnostic near-infrared (NIR) signatures, and discuss the implication of these findings for ongoing and future searches for planetary biosignatures and technosignatures.

2. Spectral Inputs and Models

Our goal is to demonstrate that at abundances consistent with climate modification, artificial greenhouse gases may be detectable in exoplanetary spectra. As a proof of concept, we examine five technosignature gases with substantial thermal infrared opacity: CF_4 , C_2F_6 , C_3F_8 , SF_6 , and NF_3 at concentrations of 1, 10, and 100 ppm in otherwise Earth-like atmospheres. This range of concentrations has been previously examined in the context of terraforming Mars (Marinova et al. 2005). We additionally examine a combination of C_3F_8 , C_2F_6 , and SF_6 in a range of 1, 10, and 100 ppm because this combination of gases more thoroughly covers the MIR window for habitable planets ($\sim 8\text{--}12$ μm ; $T_{\text{surf}} \sim 290$ K). Our base atmosphere was sourced from the Intercomparison of Radiation Codes in Climate Models (Luther et al. 1988) and represents a midlatitude summer Earth profile. The opacities for each gas were sourced from Sharpe et al. (2004) via Kochanov et al. (2019) and are shown in Figure 1. We note that only cross sections, rather than line-by-line data, are available for these gaseous species and that these data are additionally limited in wavelength coverage and precision. We examine the impact of these limitations and the need for refined opacity data for potential technosignature molecules in the Discussion section.

2.1. Planetary Spectrum Generator

To generate synthetic transmission spectra and quantify the detectability of artificial greenhouse gases in our simulated transmission spectra, we use the Planetary Spectrum Generator (PSG; Villanueva et al. 2018, 2022). PSG is a public and versatile radiative transfer tool that can be employed to simulate a wide variety of planetary environments and has been used extensively for simulating terrestrial planets, particularly the TRAPPIST-1 planetary system (e.g., Fauchez et al. 2019, 2020; Pidhorodetska et al. 2020; Suissa et al. 2020; Cooke et al. 2023; Ostberg et al. 2023). In our proof of concept transit cases, we use PSG to calculate the number of transits necessary to identify each molecule or combination of molecules investigated for a TRAPPIST-1 f test case, assuming stellar and planetary parameters sourced from NASA’S Exoplanet Archive and shown in Table 1. We simulate synthetic transmission spectra observable by JWST’s Mid-Infrared (5–12 μm) Instrument (MIRI; see Wright et al. 2004) at a constant resolving power of $R = 100$ and synthetic spectra observable by JWST’s Near-Infrared (1.5–5 μm) Spectrograph (NIRSpec; see Bagnasco et al. 2007) at a constant spectral resolution of 0.022 μm . For the NIR spectra, we note that opacity data are unavailable for CF_4 , C_2F_6 , C_3F_8 , SF_6 , and NF_3 for wavelengths shorter than 1.5 μm . Our transit calculations assume a cloud layer from 1 to 0.1 bar (i.e., an ~ 15 km tropopause) with a mass mixing ratio of 10^{-9} kg kg $^{-1}$ of ice, with an arbitrary fixed 1 μm effective radius. This cloud layer is not fully opaque and leads to a continuum level at 5.5 km.

To estimate the signal-to-noise ratio (S/N) across the NIRSpec prism and MIRI wavelength ranges and the number of transits required to achieve a 5σ detection, we proceed with the following, as in Fauchez et al. (2022): (1) we compute the spectrum without the molecule of interest; (2) we compute the spectrum with the molecule of interest; (3) we compute the difference between steps 1 and 2 across the whole instrument range; (4) we compute the S/N by dividing step 3 by the noise for one transit in each spectral interval; (5) we apply an out-of-transit factor of 1.17 to the noise assuming an out-of-transit time equal to 3 times the in-transit time; (6) the S/N of the molecule across the whole instrument range is then computed following Lustig-Yaeger et al. (2019); and (7) from the S/N, the number of transits required to achieve a 5σ detection is given as in Fauchez et al. (2019) and Fauchez et al. (2020). The noise model employed within PSG is identical to the one used in Fauchez et al. (2022) where calculations have been benchmarked with the JWST Exposure Time Calculator for both the NIRSpec prism and MIRI’s Low Resolution Spectrometer (LRS). For the NIRSpec prism, an $R = 100$ has been assumed with the SUB512S subarray with rapid readout pattern and two groups per integration (0.225 s frame $^{-1}$). For MIRI LRS, $R = 100$ has also been assumed, with the P750L disperser using the SLITLESSPRISM subarray and the FASTR1 readout pattern with 20 groups per integration (0.15 s frame $^{-1}$). The out-of-transit time has been assumed to be $1.5\times$ the in-transit time before ingress, and $1.5\times$ after egress, therefore leading to an out-of-transit baseline 3 times longer than the in-transit time. We uploaded our planetary spectra within PandExo¹⁰ to compute the transit depth uncertainty per spectral interval for one transit as shown in Appendix A. The transit depth uncertainty increases

¹⁰ <http://exoctk.stsci.edu/pandexo>

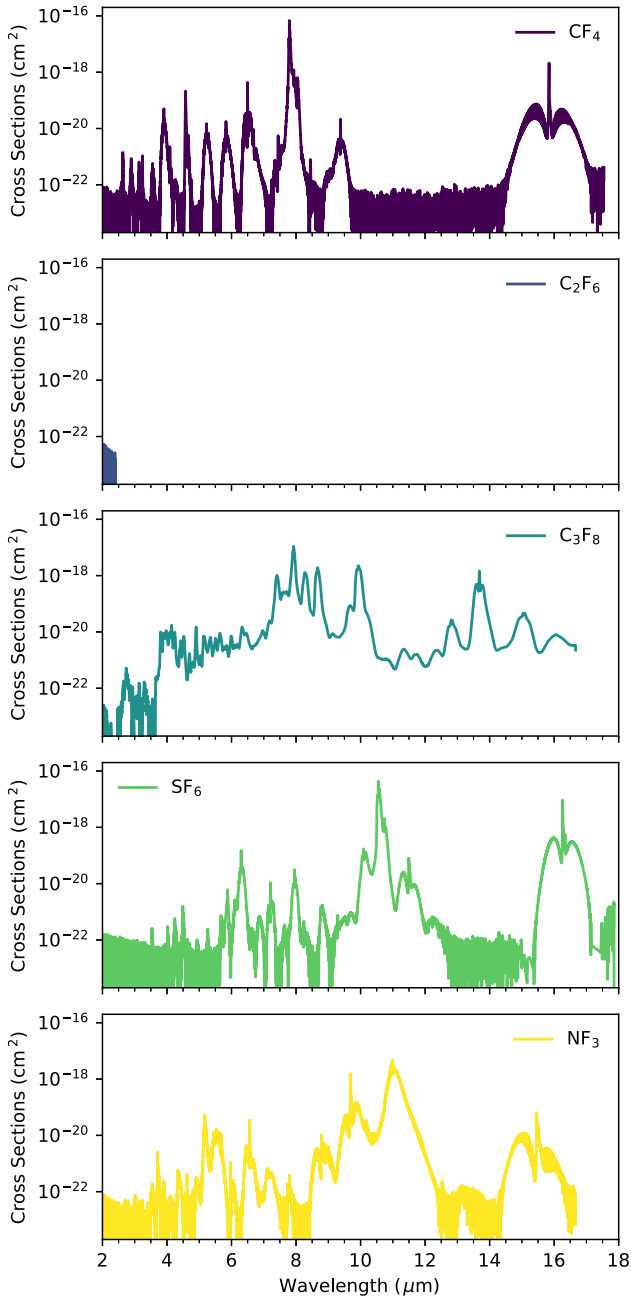


Figure 1. Infrared (2–18 μm) cross sections for the atmospheric technosignature molecules examined in this study, which include CF_4 , C_2F_6 , C_3F_8 , SF_6 , and NF_3 . Data are sourced from Sharpe et al. (2004) and Kochanov et al. (2019).

dramatically beyond 5 μm for the NIRSPEC prism detector. Any absorption features beyond that value would therefore be more detectable with MIRI LRS.

2.2. SMART

To generate synthetic emission spectra, we use the Spectra Mapping Atmospheric Radiative Transfer (SMART) model (Meadows & Crisp 1996; Crisp 1997). SMART is a 1D line-by-line, multistream, multiple-scattering radiative transfer model that is well validated by observations of Earth and solar system bodies (Tinetti et al. 2005; Robinson et al. 2014a, 2014b; Arney et al. 2014) and is often used to simulate the

Table 1
TRAPPIST-1 System Properties Modeled

Parameter	Value
TRAPPIST-1	
Distance (pc)	12.4
Spectral type	M8V
T_{eff} (K)	2566
Mass (M_{\odot})	0.0898
Radius (R_{\odot})	0.12
TRAPPIST-1 f	
Semimajor axis (au)	0.03849
Mass (M_{\oplus})	1.039
Radius (R_{\oplus})	1.045
Orbital period (days)	9.2075
Transit duration (hr)	1.05
Inclination (deg)	89.74
Irradiation (S_{\oplus})	0.349
Density (g cm^{-3})	5.042
Surface gravity (m s^{-2})	9.37

spectra of exoplanet atmospheres (e.g., Charnay et al. 2015; Lustig-Yaeger et al. 2023a). SMART uses the HITRAN line lists (Gordon et al. 2022) to calculate the opacities of major molecules using its companion program LBLABC, with the exception of the artificial gas cross-section data as described above. Our emission spectra assume a planet that has an identical surface gravity and radius as the Earth, in contrast to the TRAPPIST-1 f transit scenario described above. We simulate planetary emission from 5–21 μm at 1 cm^{-1} resolution with SMART, but these spectra are down-binned for S/N calculations with LIFESIM as described below. As this is a first-pass look at the potential detectability of artificial greenhouse gases, we neglect cloud cover in our emitted light spectral simulations and assume a surface emissivity of 1.

2.3. LIFESIM

LIFE (Kammerer & Quanz 2018; Quanz et al. 2022) is a mission concept for a large, space-based, formation-flying, MIR, nulling interferometer observatory for the direct detection and atmospheric characterization of a large sample of terrestrial, potentially habitable exoplanets. ESA’s Voyage 2050 Senior Committee report¹¹ recommended “the characterization of the atmosphere of temperate exoplanets in the mid-infrared” with “highest scientific priority” as a candidate topic for a future L-class mission in the ESA Science Programme. LIFE directly addresses this scientific theme. Typical observational cases for LIFE will be planets in the habitable zone of M stars at ~ 5 pc, and “Sun-like” FGK stars at ~ 10 pc (Dannert et al. 2022; Kammerer et al. 2022).

We use the LIFESIM software designed for LIFE to calculate the resulting detectability of features present in our simulated SMART-generated emission spectra using the same methods as described in Angerhausen et al. (2023). The current version of LIFESIM includes astrophysical noise sources, including stellar leakage and thermal emission from local zodiacal and exozodiacal dust. The software is designed to be flexible, allowing for the incorporation of instrumental noise terms in future iterations. An important feature of LIFESIM is its ability to provide a user-friendly means of predicting the expected S/N for future LIFE observations by considering various instrument

¹¹ <http://www.cosmos.esa.int/web/voyage-2050>

Table 2
Overview of the Simulation Parameters Used in LIFESIM

Parameter	Value
Quantum efficiency	0.7
Throughput	0.05
Minimum wavelength	4 μm
Maximum wavelength	18.5 μm
Spectral resolution	50
Interferometric baseline	10–100 m
Apertures diameter	2 m
Exo-zodiacal dust	$3 \times$ local zodiacal dust

Note. These are the same LIFE baseline values as those used in Quanz et al. (2022) or Angerhausen et al. (2023).

and target parameters. Further details can be found in Dannert et al. (2022).

The LIFESIM configuration for the presented output spectra followed the current LIFE “baseline” setup, featuring four apertures of 2 m diameter each, a broadband wavelength range spanning 4–18.5 μm , a throughput of 5%, and a spectral resolution set at $R = 50$. During the simulation, we assume an exo-zodiacal level equivalent to 3 times the local zodiacal density for the characterization observations. This assumption aligns with the findings of the HOSTS survey, which predicted the expected median emission level (as detailed in Ertel et al. 2020). The nulling baseline setup ranged from 10 to 100 m (this assumes prior knowledge of the planets through other surveys or detection in the LIFE detection phase, allowing for baseline optimization in each case). An overview of the LIFESIM simulation parameters is given in Table 2. For each case, we assumed the planet in the outer continuous habitable zone, specifically, at an orbital distance for which the solar constant is 0.53.

As in Angerhausen et al. (2024), we give two metrics for detectability: maximum difference in one band in units of sigma and the band-integrated S/N defined as:

$$(S/N)_{\text{band}} = \sqrt{\sum_{i=1}^n \left(\frac{\Delta y_i}{\sigma(y_i)} \right)^2}, \quad (1)$$

where Δy_i is the difference between the spectrum containing the technosignature feature and a spectrum that does not in each of the n spectral bins and $\sigma(y_i)$ is the LIFE sensitivity in the respective bin. More detailed studies would also include retrievals (Alej et al. 2022; Konrad et al. 2022), but we have shown that the qualitative detectability criteria used here translate well for quantitative retrievals (Angerhausen et al. 2024).

3. Synthetic Planetary Spectra Results

Here we describe the resulting synthetic planetary emission spectra for the artificial greenhouse gas scenarios described in Section 2. Where applicable, we quantified the relative detectability of these gas features with JWST and LIFE.

3.1. Transmission Spectra in the Mid-infrared

Figure 2 shows the resulting MIR (5–12 μm) transmission spectra of a hypothetical TRAPPIST-1 f and the various concentrations of the technosignature gases listed above. This

wavelength region lies within the range of MIRI’s LRS. We draw attention to the fact that even at 1 ppm, every technosignature gas produces maximum transmission depths that rival or exceed those of the 9.65 μm O₃ band, which is included within the plotted range. The PFC gases (CF₄, C₂F₆, and C₃F₈) contribute to discrete absorption maxima at several wavelengths. The strongest feature of C₄ is located at $\sim 7.9 \mu\text{m}$, with additional significant features at 5.25, 5.9, 6.5, and 9.2 μm . Each of these features spans $\gtrsim 0.02 \mu\text{m}$, depending on concentration. In contrast, C₂F₆ and C₃F₈ have more numerous features throughout the MIR that blend together at high concentration (potentially as a result of uncertainties in the input opacities, see the Discussion section), and much stronger absorption at wavelengths 8–9 μm . C₃F₈ additionally possesses a strong feature at $\sim 9.9 \mu\text{m}$. The strongest feature of SF₆ lies at $\sim 10.7 \mu\text{m}$ with weaker features at 5.8, 6.3, 6.9, 7.2, 8.0, 8.8, and 11.4 μm . A combination of C₃F₈, C₂F₆, and SF₆ is thus strongly absorptive throughout the entire MIR region shown, particularly at higher greenhouse gas concentrations. We also examine NF₃, which has its strongest feature located at 11 μm , which is substantial at even 1 ppm. It also has weaker features at 5.2, 5.6, 6.5, 7.2, 8.8, and 9.8 μm . Simulated data points for the 100 ppm technosignatures gases, using 10 transits at $R = 50$, show a clear deviation from the black MIR spectrum with no technosignature gases.

In Table 3, we show the number of transits needed to detect each technosignature gas and gas combination at 5σ on each simulated TRAPPIST-1 f with MIRI LRS according to the procedure described in Section 2.1. The combination of C₂F₆, C₃F₈, and SF₆ can be detected in five transits at 100 ppm and 10 transits at 10 ppm. In each scenario, the number of transits required to detect any of these technosignature gases at ≥ 1 ppm concentration is orders of magnitude lower than for O₃ or CO₂, which are effectively undetectable with MIRI. We note that while uniquely retrieving the identities of these terraforming gases would likely require further characterization (see the Discussion), these results illustrate that unexpected MIR opacities consistent with a terraformed atmosphere, as simulated here, and are within the observational capabilities of JWST.

3.2. Transmission Spectra in the Near-infrared

Figure 3 shows simulated NIR (1.5–5 μm) spectra of TRAPPIST-1 f with 1, 10, and 100 ppm of C₂F₆, C₃F₈, SF₆, and an equal combination of the three. Notably, C₂F₆ and C₃F₈ produce substantial absorption features comparable to or greater than CO₂ at concentrations ≥ 10 ppm. These two gases produce substantial absorption features in the 4–5 μm region that overlap with the 4.3 μm CO₂ band and the 4.8 μm O₃ band, but are much broader. In addition, a weaker band near 2.8 μm is apparent at high concentrations (~ 100 ppm) that overlaps with a separate CO₂ band. In contrast, the NIR features caused by SF₆ are muted and only apparent at concentrations $\gtrsim 10$ ppm. Even at 100 ppm concentrations of SF₆, its NIR spectral features are extremely limited when compared to those of CO₂. The combined NIR spectra are dominated by features from C₂F₆ and C₃F₈. Simulated data points for the 100 ppm technosignatures gases, using 10 transits at $R = 10$, again show a clear deviation from the black NIR spectrum with no technosignature gases.

We calculate the single transit S/N and the number of transits needed to detect these gases with JWST NIRSpec at 5σ

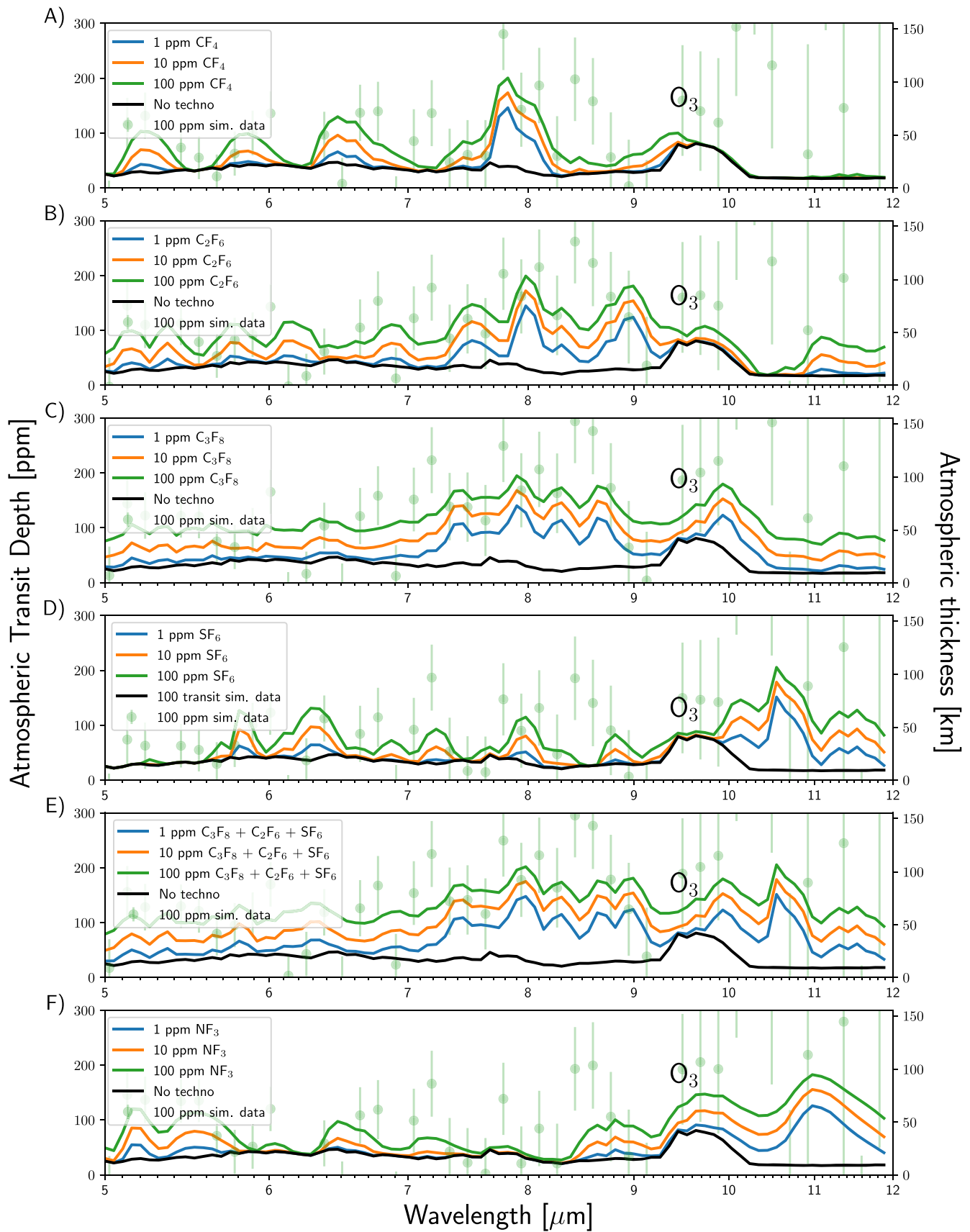


Figure 2. PSG-simulated MIR (5–12 μm) transmission spectra of an Earth-like TRAPPIST-1 f with 1–100 ppm of technosignature gases CF_4 (A), C_2F_6 (B), C_3F_8 (C), SF_6 (D), a combination of the preceding three gases (E), and NF_3 (F). Simulated data points for the 100 ppm cases are shown in green, for 10 transits and at a resolving power of $R = 50$ for clarity.

Table 3Number of Transits Required to Reach a 5σ Detection (5σ Transit) with MIRI LRS for a Given Modeled Atmosphere

Atmosphere	5σ Transit
100 ppm	
$C_2F_6 + C_3F_8 + SF_6$	5
C_2F_6	6
C_3F_8	8
SF_6	19
NF_3	16
10 ppm	
$C_2F_6 + C_3F_8 + SF_6$	10
C_2F_6	13
C_3F_8	20
SF_6	57
NF_3	52
1 ppm	
$C_2F_6 + C_3F_8 + SF_6$	25
C_2F_6	38
C_3F_8	60
SF_6	>100
NF_3	>100
Molecular Comparison	
Earth-like O_3	>100
378 ppm CO_2	>100

in Table 4, again following the procedure described in Section 2.1. We find that the combination of all three gases is potentially detectable in as few as four transits if all are present at 100 ppm concentrations and as few as 14 transits at 10 ppm. Individually, each technosignature gas is less detectable, with SF_6 alone being functionally undetectable in the NIR with NIRSpec at any concentration ≤ 100 ppm. However, at 100 ppm, C_2F_6 and C_3F_8 could be detected in around ~ 40 transits, which is similar to the number of transits needed to detect 100 ppm of CO_2 . Overall, we find a similar number of transits are required to detect these artificial greenhouse gases at high concentrations (~ 100 ppm) in both the NIR and MIR, but there is an advantage to MIR observations in detecting intermediate concentrations (~ 1 –10 ppm). It is likely that access to both wavelength regimes would aid in full retrievals.

3.3. Emission Spectra in the Mid-infrared

We show the simulated emission spectra of Earth-twin planets with artificial greenhouse gases CF_4 , C_2F_6 , C_3F_8 , SF_6 , and NF_3 in Figure 4 assuming concentrations of 1, 10, and 100 ppm as we did for the transit transmission cases presented in Section 3.1. We further break out the scenarios with combinations of 1, 10, and 100 ppm each of $C_3F_8 + C_2F_6 + SF_6$ in Figure 5. The strongest apparent gases in emission will differ from those in transmission because the absorption depths depend not only on the concentration of the absorbing gas, but also the surface temperature of the planet, the temperature structure of the planet’s atmosphere, and the interference with other absorbing gases that manifest differently in emission versus transit transmission (e.g., H_2O). We note here that even at 1 ppm, several of these technosignature gases, including C_2F_6 , C_3F_8 , and SF_6 , display

strong MIR absorption features that equal or exceed that of O_3 at $9.65 \mu m$.

CF_4 has relatively weak features at 1 ppm, but substantial absorption at 7.9 and $9.2 \mu m$ at concentrations ≥ 10 ppm. As in transmission, C_2F_6 produces strong features from 8 to $9 \mu m$. At 100 ppm, C_2F_6 produces an additional strong feature near $11 \mu m$. C_3F_8 has strong features throughout the 8–12 μm window region that are particularly strong from 8 to $10 \mu m$. Furthermore, as seen in transit, SF_6 features are most prominent from 10 to $12 \mu m$, with one strong feature at $8.8 \mu m$ apparent at 100 ppm. NF_3 has a strong feature at $11 \mu m$ apparent even at 1 ppm, with broad absorption from 10 to $12 \mu m$ at 10 ppm, and throughout the entire 8–12 μm window at concentrations of 100 ppm. At 100 ppm, some gases, such as CF_4 and SF_6 , can show emission features because high optical depths are reached in the warm stratosphere. We note that the temperature structure is based on modern Earth, as described in Section 2. We describe the possible benefit of self-consistent calculations, and why they may not yet be possible, in Section 4. We quantify the detectability of these artificial greenhouse gas signatures with a hypothetical MIR direct-imaging observatory in the subsection below.

3.3.1. Mid-infrared Observations with a LIFE-like Observatory

Tables 5 and 6 show the results for simulated LIFE observations with various combinations of host stars, technosignature gas combinations, stellar distances, and observation times. Figure 6 shows some exemplary cases including different stellar host star types (M8V, K6V, and G2V), distances (5–10 pc), and integration times (10–50 days). Maximum channel and band-integrated S/Ns are calculated according to the methodology given in Section 2.3. Virtually all cases seem to be observable (i.e., spectral features are detectable at or above the 5σ level) at typical observation times between 10 and 50 days, much less time than needed for the detection of typical biosignature gases such as O_3 at $9.65 \mu m$ (Alej et al. 2022; Konrad et al. 2022; Angerhausen et al. 2023, 2024). First hints at the presence of additional, unusual MIR absorbers would probably already be found after relatively short preliminary observations. These results indicate that an MIR instrument is the ideal choice to observe civilizations that manipulate their climates and that tests for these technosignature gases are essentially “free” since evidence for these features would be found even before typical biosignature gases become detectable. We provide an extended table of calculations for the detectability of 1, 10, and 100 ppm of SF_6 , C_2F_6 , C_3F_8 , NF_3 , and CF_4 applied to each host star (G2V, K6V, and M8V), distance (5 and 10 pc), and integration time (10 and 50 days) in Appendix B, Table 6.

4. Discussion

4.1. Detectability of Artificial Greenhouse Gases

We have shown here that synthetic molecules previously proposed as potential terraforming gases on Mars (e.g., Marinova et al. 2005; Dicaire et al. 2013) can be detected on terrestrial exoplanets with JWST or a large, space-based MIR direct-imaging interferometer such as the LIFE concept (e.g., Kammerer & Quanz 2018) at the reasonable abundances necessary to impart a substantial climatic effect (i.e., $\gtrsim 1$ ppm in a 1 bar atmosphere). Specifically, we have shown that CF_4 , C_2F_6 , C_3F_8 , SF_6 , and NF_3 , alone and in combination, can

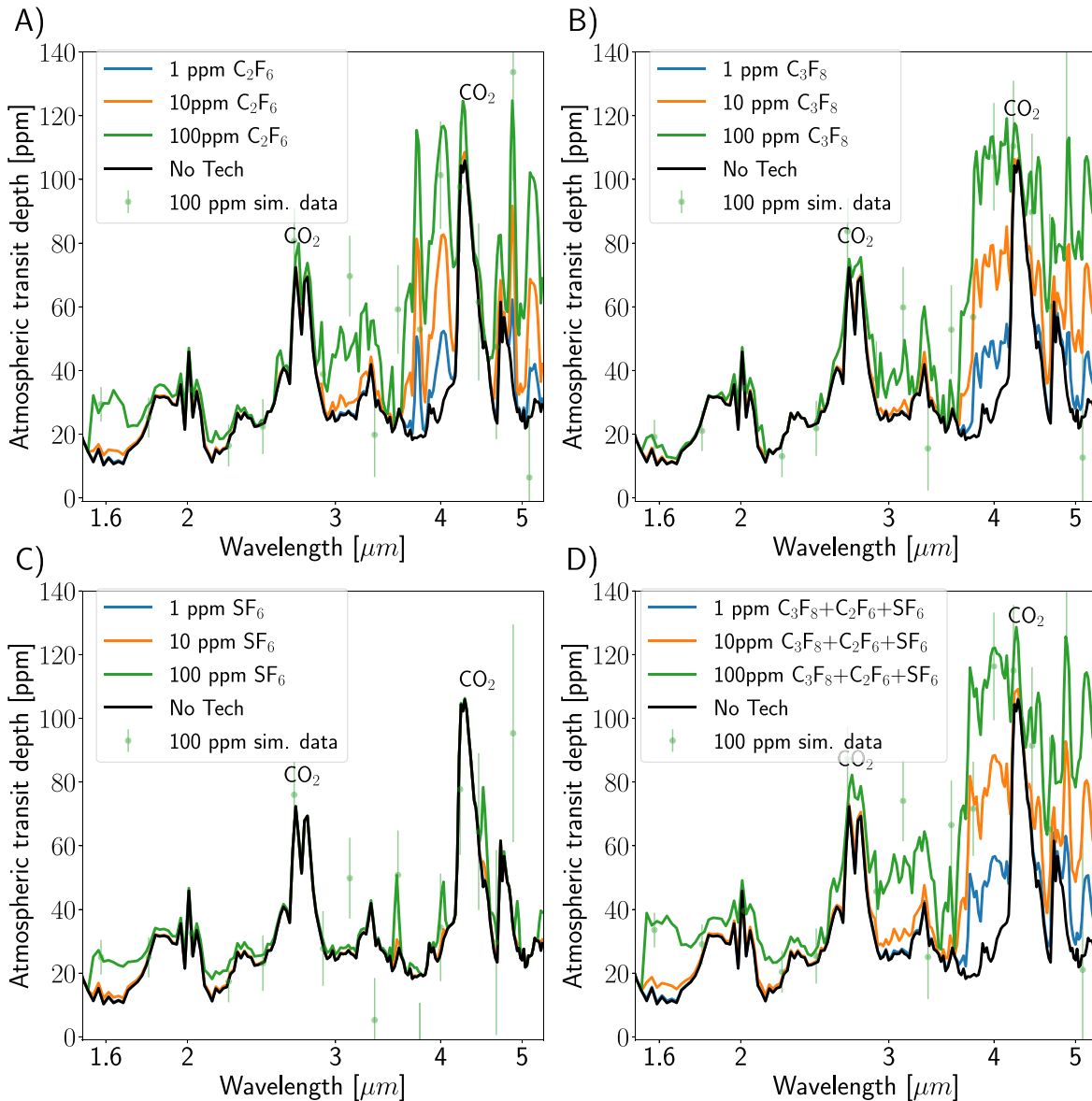


Figure 3. PSG-simulated NIR (1.5–5 μm) transmission spectra of the modeled TRAPPIST-1 f atmospheres with 1, 10, and 100 ppm of technosignature gases C_2F_6 (top left), C_3F_8 (top right), SF_6 (bottom left), and a combination of the preceding three gases (bottom right). Simulated data points for the 100 ppm cases are shown in green, for 10 transits and at a resolving power of $R = 10$ for clarity.

produce MIR (5–12 μm) transit signatures comparable to or greater than the 9.65 μm O_3 band at concentrations $\gtrsim 1$ ppm (Figure 2). We calculated the number of transits required to detect C_2F_6 , C_3F_8 , SF_6 , NF_3 , and equal combinations of the first three gases at 1, 10, and 100 ppm on TRAPPIST-1 f with MIRI LRS and found surprisingly few transits are required, as few as five for a 5σ detection for a combination of each gas at 100 ppm, and 10 transits for the same at 10 ppm (Table 3). Of the gases individually, C_2F_6 is the most detectable at any given concentration, while C_3F_8 is still strongly detectable, and SF_6 requires the most number of transits to be detected at any given concentration. NF_3 requires slightly fewer transits to detect than SF_6 (e.g., 16 versus 19 at 100 ppm). Nonetheless, SF_6 and NF_3 are still much more detectable than O_3 or CO_2 in an Earth-like atmosphere at concentrations > 1 ppm.

We repeated the above analysis in the NIR (1.5–5 μm) and calculated the number of transits required to detect each of the three gases (C_2F_6 , C_3F_8 , and SF_6) alone or in combination on

TRAPPIST-1 f with JWST NIRSpec (Figure 3 and Table 4). We found that at concentrations of 100 ppm, a combination of all three gases can be detected in as few as four transits, and at 10 ppm in as few as 14 transits. However, each gas individually is far less detectable than the corresponding MIR case. While C_2F_6 and C_3F_8 produce spectral signatures comparable to CO_2 at 100 ppm, SF_6 alone is likely not reasonably detectable at concentrations ≤ 100 ppm. Both our mid and NIR analyses of the detectability of these technosignature gases in transit compare favorably with past predictions for biosignature detectability on the TRAPPIST-1 planets. For example, multiple studies have found that the CH_4 – CO_2 disequilibrium pair could be detected on an Archean-Earth-like TRAPPIST-1 e in ~ 10 transits (Krissansen-Totton et al. 2018a; Mikal-Evans 2021; Meadows et al. 2023), while we find that potentially even fewer transits would be required to detect C_2F_6 or C_3F_8 at 100 ppm, or in combination ($\text{C}_2\text{F}_6 + \text{C}_3\text{F}_8 + \text{SF}_6$) at 10 ppm. Moreover, these aforementioned studies find that detecting

Table 4
Number of Transits Required to Reach a 5σ Detection (5σ Transit) with NIRSpec for a Given Modeled Atmosphere

Atmosphere	5σ Transit
100 ppm	
$C_2F_6 + C_3F_8 + SF_6$	4
C_2F_6	36
C_3F_8	41
SF_6	>100
100 ppm CO_2	48
378 ppm CO_2	25
10 ppm	
$C_2F_6 + C_3F_8 + SF_6$	14
C_2F_6	>100
C_3F_8	83
SF_6	>100
1 ppm	
$C_2F_6 + C_3F_8 + SF_6$	80
C_2F_6	>100
C_3F_8	>100
SF_6	>100

biogenic O_2 and O_3 may not be possible on the TRAPPIST-1 planets, while we find a range of scenarios that would allow detection of artificial greenhouse technosignature gases at concentrations of ~ 1 ppm.

We also calculated the MIR emitted light spectra for an Earth-twin planet with 1, 10, and 100 ppm of CF_4 , C_2F_6 , C_3F_8 , SF_6 , and NF_3 (Figure 4) and the corresponding detectability of C_2F_6 , C_3F_8 , and SF_6 with the LIFE concept mission (Figure 6 and Table 5). We find that in every case, the band-integrated S/Ns were $>5\sigma$ for outer habitable zone Earths orbiting G2V, K6V, or TRAPPIST-1-like (M8V) stars at 5 and 10 pc and with integration times of 10 and 50 days. Importantly, the threshold for detecting these technosignature molecules with LIFE is more favorable than standard biosignatures such as O_3 and CH_4 at modern Earth concentrations, which can be accurately retrieved (Alej et al. 2022; Angerhausen et al. 2024), indicating meaningfully terraformed atmospheres could be identified through standard biosignatures searches with no additional overhead.

4.2. Fingerprinting Artificial Greenhouse through Infrared Anomalies

In principle, the abundances of technosignature molecules can be retrieved from transit transmission or MIR direct-imaging spectroscopy. For example, Lustig-Yaeger et al. (2023b) retrieve CFC-11 (CCl_3F) and CFC-12 (CCl_2F_2) abundances from reconstructed Earth transit spectra from the Canadian low-Earth orbit satellite SCISAT (Macdonald & Cowan 2019). However, as shown here, high concentrations of artificial greenhouse gases can act to fill the entire MIR window, blending features and potentially interfering with our ability to uniquely identify absorbing gas species (though a full exploration of every possible permutation is beyond the scope of this work). Indeed, an extraterrestrial civilization may be motivated to precisely optimize and calibrate a combination of artificial greenhouse gases to fill the MIR window and maximize warming potential at the lowest cost (see the related discussion as applied to terraforming Mars in, e.g., Marinova et al. 2005). In such a scenario, it may be difficult to uniquely

identify and constrain the abundance of each contributing gas. However, in any case, meaningful radiative forcing necessitates high infrared opacity in the window region, which would be apparent in transit or emission spectroscopy. We propose that anomalously large MIR transit signatures or anomalously low infrared emission could serve as “first-pass” indicators of terraformed planets (see the concept illustrations in Figure 7). For transmission observations, the artificial nature of this anomalous absorption could be confirmed via higher-S/N MIR observations that would reveal individual molecular features, or diagnostic NIR features that would not be optimized for climatic impact. In emission spectra, higher-S/N observations may reveal features within the window, particularly at the wings of the strongest absorption features, which may show higher brightness temperatures than near the center.

MIR searches are important complements to biosignature searches in the UV/visible/NIR range because some gaseous species such as CH_4 and N_2O (and O_3 if we neglect the UV) are more detectable via MIR observations at Earth-like concentrations (e.g., Alej et al. 2022; Konrad et al. 2022; Schwieterman et al. 2022; Angerhausen et al. 2024). Moreover, due to inner-working angle constraints, an NIR/visible/UV surveyor, such as the proposed Habitable Worlds Observatory (HWO), is most capable of characterizing habitable zone planets around Sun-like stars (LUVOIR-Team 2019). While the proposed LIFE mission is similarly well suited to detect and characterize “Earth twins” in synergy with HWO, it also has a unique discovery space in the habitable zones of late type stars [i.e., K and M versus G and F] due to its long baselines, which translate into very high spatial resolution (see, e.g., Carrión-González et al. 2023). Given the impetus to characterize temperate rocky exoplanets in the MIR to search for signs of habitability and life, a commensal search for artificial greenhouse gases on the same targets would not impose further costs (NASA Technosignatures Workshop Participants 2018; Haqq-Misra et al. 2022b), and could reveal these signatures if their absorption features are comparable to the habitability markers that are sought by biosignature searches. We quantitatively demonstrate that these features are indeed comparable or exceed those of standard biosignature gases at abundances ≥ 1 ppm.

4.3. The Case for Long-lived, Low-toxicity Greenhouses Gases as Compelling Planetary Technosignatures

As mentioned in the Introduction, a civilization may be motivated to modify the climate of a planet to forestall imminent global cooling on their home world, or to terraform an otherwise uninhabitable planet within their system (or beyond), as humans have proposed to do with Mars. Alternatively, a civilization may seek to reduce the amount of CO_2 necessary to warm an already habitable planet in the outer habitable zone, which could require several bars of CO_2 to remain clement (Kopparapu et al. 2013; Shields et al. 2016; Schwieterman et al. 2019). For example, Fauchez et al. (2019) find that 1–10 bars of CO_2 is required to warm the surface of TRAPPIST-1 f or g. These levels of CO_2 impose substantial physiological challenges on complex aerobic organisms (e.g., Schwieterman et al. 2019; Ramirez 2020), so while these environments may be “habitable” to microbes, it does not necessarily follow that they would be suitable for higher forms of organic life. The radiative forcing otherwise provided by massive amounts of CO_2 could instead be provided by

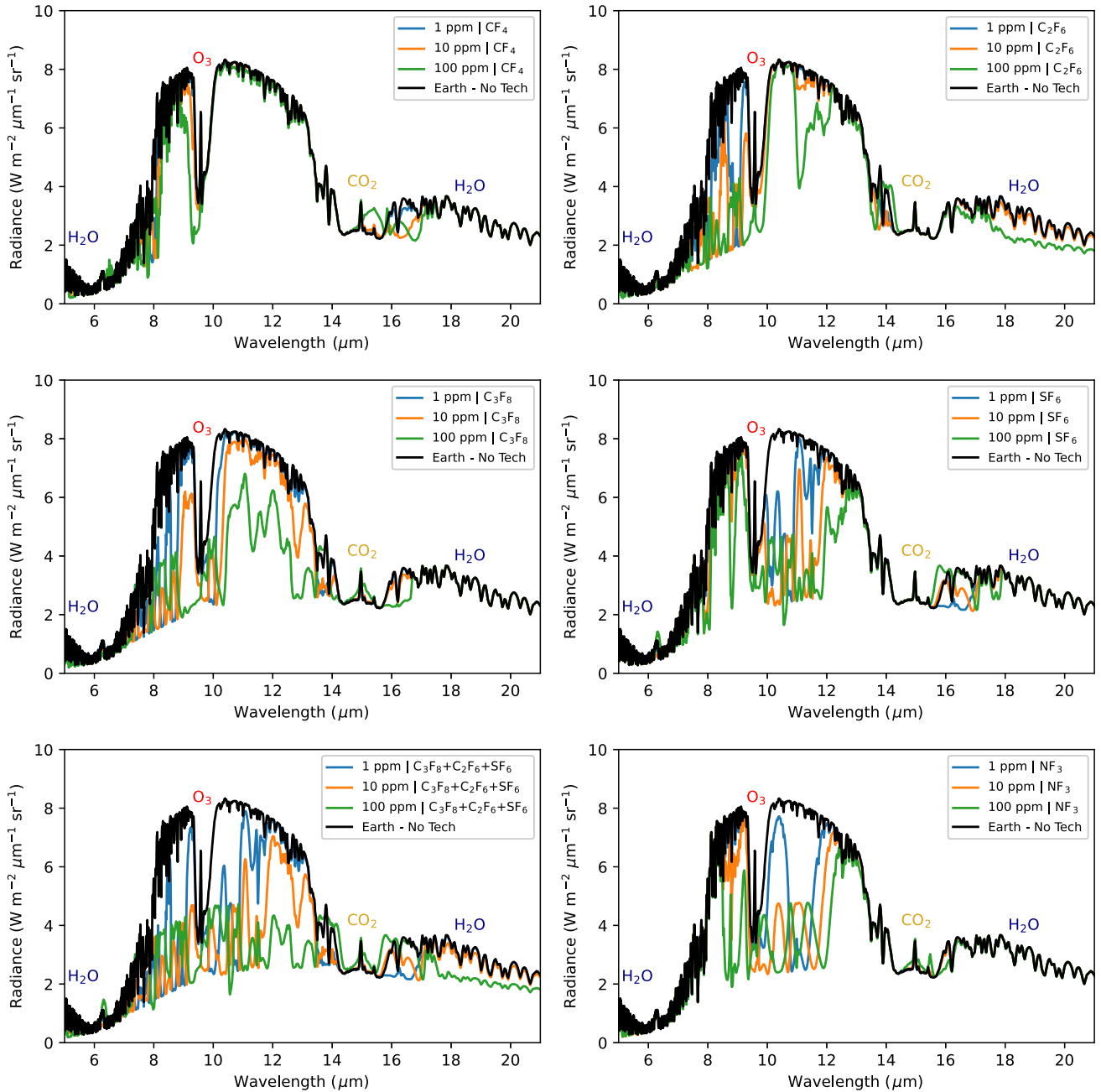


Figure 4. SMART-simulated MIR (5–21 μm) emission spectral radiances of an Earth-twin planet with 1–100 ppm of technosignature gases CF_4 (top left), C_2F_6 (top right), C_3F_8 (middle left), SF_6 (middle right), a combination of the preceding three gases (bottom left), and NF_3 (bottom right).

alternative molecules that more effectively absorb within the MIR window (8–12 μm), a wavelength range that is predetermined by the blackbody peak of a habitable planetary surface (e.g., ~ 300 K).

Fluorine-bearing gases including PFCs (e.g., CF_4 , C_2F_6 , and C_3F_8), SF_6 , and NF_3 have been proposed as artificial greenhouse gases for terraforming Mars for multiple reasons, including their high MIR opacity, long atmospheric lifetimes, reduced reactivity with atmospheric O_3 , and low toxicity to life due to their chemical inertness (Marinova et al. 2005). On a molecule-per-molecule basis, the radiative forcing of the artificial greenhouse gases explored here are orders of magnitude greater than CO_2 , and so bars of CO_2 could hypothetically be replaced by a much smaller atmospheric

loading of these technosignature gases (Marinova et al. 2005). For example, the global warming potential (GWP) of C_2F_6 is on the order of 10,000 times that of CO_2 on a 100 yr timescale (see Table 1 in Mühle et al. 2010). SF_6 has a 100 yr GWP of 23,500 (Myhre et al. 2013).

These gases are primarily produced on Earth today in small quantities as a by-product of industrial processes. SF_6 is manufactured as an insulator and has a modern atmospheric concentration of 11 ppt (Lan et al. 2023). It has a lifetime of approximately ~ 1000 yr, though estimates vary by a few hundred years, and is primarily destroyed in the ionosphere via collisions with energetic electrons (Kovács et al. 2017; Ray et al. 2017). PFCs are produced primarily as a by-product of aluminum smelting and semiconductor production and have

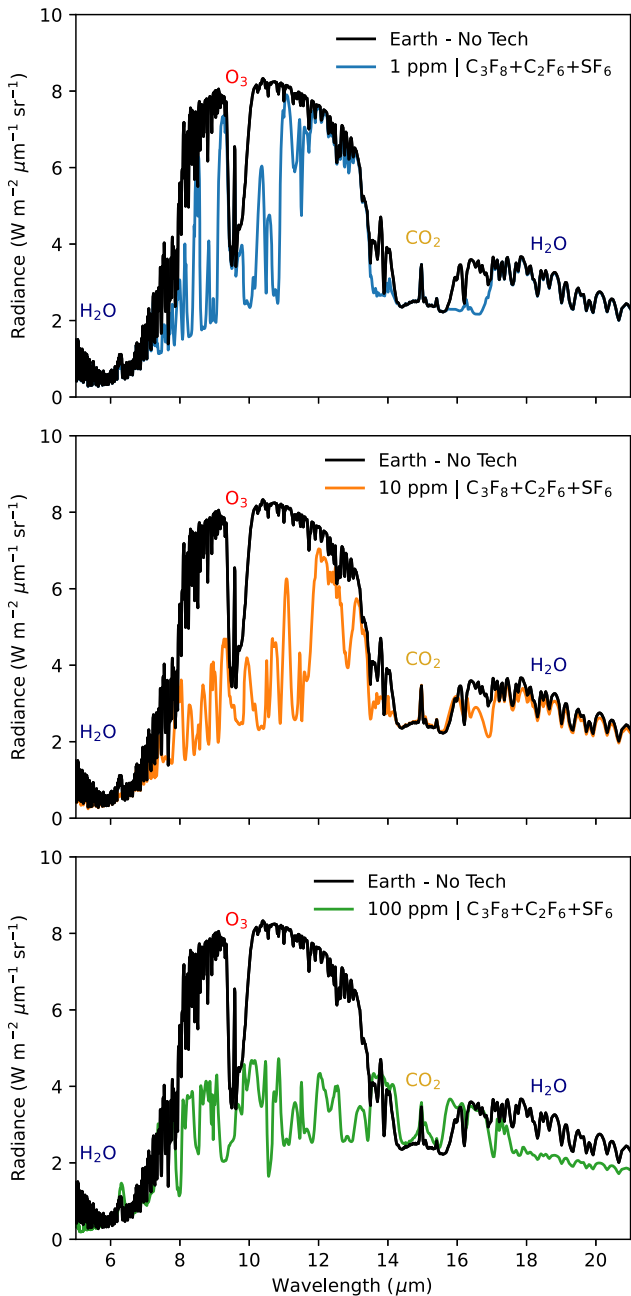


Figure 5. Similar to Figure 4, but breaking out SMART-simulated emission spectra with combinations of $C_3F_8 + C_2F_6 + SF_6$ each of which with concentrations of 1 ppm (top panel), 10 ppm (middle panel), and 100 ppm (bottom panel). The Earth without technosignature gases is shown for comparison in each panel (black line).

atmospheric lifetimes of $\sim 2000\text{--}50,000$ yr (Mühle et al. 2010), and modern concentrations of 87 ppt (CF_4), 5 ppt (C_2F_6), and 0.7 ppt (C_3F_8 ; Prinn et al. 2018a, 2018b). PFCs are destroyed by molecule-ion reactions in the ionosphere (Lodders & Fegley 2015). NF_3 has been used as a replacement for PFCs in circuit etching and other chemical processes, but has an atmospheric lifetime of 1020 yr and a GWP of 7370 (Maione et al. 2013; Totterdill et al. 2016). It has a modern concentration of 2.5 ppt (Prinn et al. 2018a, 2018b). While the concentrations of these gases are small, their high GWP values make these gases important targets for emission reduction to arrest the worst

impacts of global climate change (e.g., Illuzzi & Thewissen 2010).

The vast majority of these gases present in the modern atmosphere have been produced via anthropogenic activity, though small abiotic sources exist. CF_4 and SF_6 are produced via the weathering of fluorite-bearing minerals and have measured preindustrial background concentrations of ~ 35 and ~ 0.01 ppt based on ice core samples (Harnisch & Eisenhauer 1998; Mühle et al. 2010). The preindustrial concentrations of C_2F_6 , C_3F_8 , and NF_3 are either small (< 0.01 ppt) or nonexistent (Arnold et al. 2013; Trudinger et al. 2016). In addition to low-abiotic sources, Seager et al. (2023) argue that fully fluorinated NF_3 and SF_6 are unlikely to be made biologically (by nontechnological life) because of life’s aversion to using fluorine except in limited circumstances and is not known to produce fully fluorinated volatile gases. See also a related discussion of the likelihood of fluorine-bearing gaseous biosignatures in Section 5.2 of Leung et al. (2022).

While all technosignature scenarios are speculative, we argue that it is unlikely fluorine-bearing technosignature gases will accumulate to detectable levels in a technosphere due only to inadvertent emission of industrial pollutants (or volcanic production), and that our best opportunity to detect them likely requires their use at higher abundances for the intentional modification of a planet’s climate. These gases exist at parts-per-trillion levels on Earth’s atmosphere, which are undetectable over interstellar distances with near or intermediate future telescopes, and yet nonetheless meaningfully contribute to our civilizational challenge of global climate change because of their large GWP values. PFCs, SF_6 , and NF_3 are regulated by the UN Framework Convention on Climate Change (UNFCCC) with reporting requirements for all member nations (UNFCCC COP 19, 2013). These concentrations are approximately 6 orders of magnitude smaller than those we examine in this work. However, as argued above and in our Introduction, purposeful climate modification (including terraforming of otherwise nonhabitable planets) provides a plausible motivation for a technological civilization to maintain large concentrations of artificial fluorine-bearing greenhouse gases over long timescales.

4.4. Limitations of Current Work and Need for Refined Opacities

We presented first-pass simulations of artificial greenhouse gases at prescribed mixing ratios (1, 10, and 100 ppm in a 1 bar atmosphere). We did not simulate self-consistent climates, which could be an important consideration for future work. Planetary climate will depend on numerous factors including instellation, surface albedo, cloud composition and cloud coverage, total atmospheric pressure, mixing ratios of nontechnosignature gases, surface water availability, and many more. It is beyond the scope of this work to analyze the effect of each of these variables on technosignature gas detectability, however, we will briefly note below future areas for improvement.

In our transmission spectra, our clouds are prescribed, rather than self-consistent, which could lead to differences in the lower atmosphere corresponding to smaller transit depths. However, because the transit altitudes for artificial greenhouse gases are far above the troposphere (~ 15 km), the impact on our results will be minimal. Fauchez et al. (2019) find that the transits needed to detect CH_4 , CO_2 , and O_3 on TRAPPIST-1 f

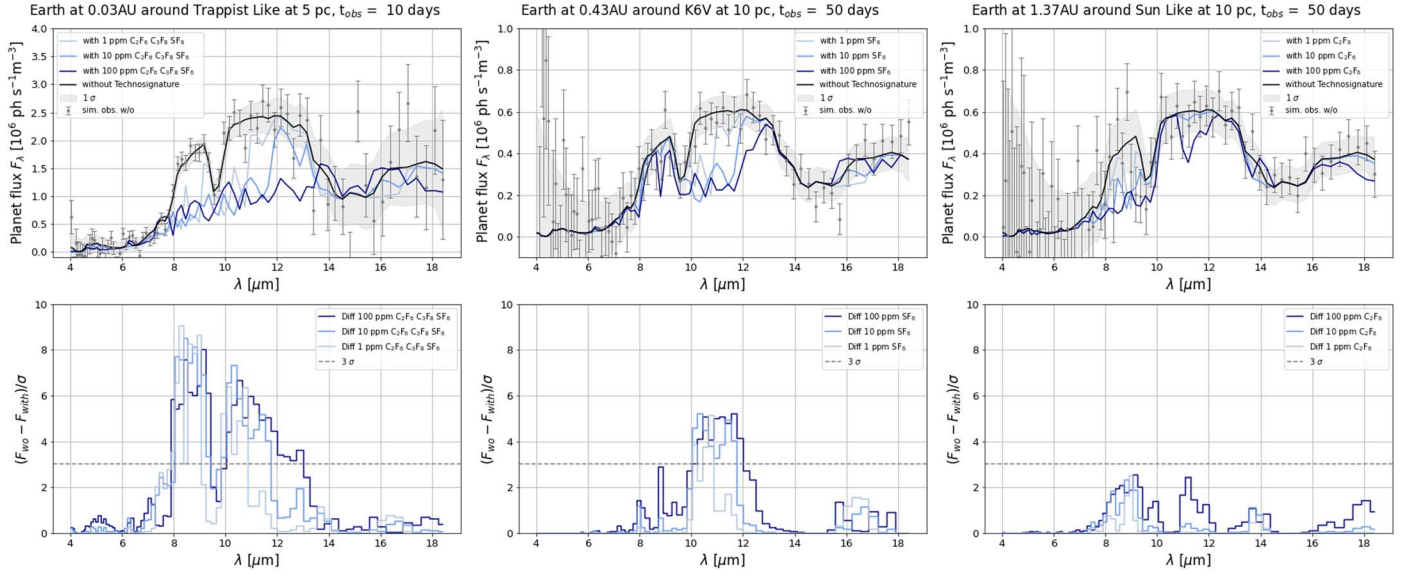


Figure 6. Three LIFE example artificial greenhouse gas detection cases (parameters in the titles). From left to right: least challenging (TRAPPIST-1-like host at 5 pc, 10 days, a combination of three technosignature gases), average (K6V host at 10 pc, 50 days, SF_6 only), and most challenging (Sun-like host at 10 pc, 50 days, C_2F_6 only). Top: planet flux for atmospheres with and without the feature. The gray area represents the 1σ sensitivity; the gray error bars show an individual simulated observation. Bottom: statistical significance of the detected differences between an atmospheric model with and without the technosignature gas(es).

Table 5
Detectability of the $\text{C}_2\text{F}_6 + \text{C}_3\text{F}_8 + \text{SF}_6$ Combination of Technosignature Gases with LIFE

Host Star	Distance	T_{obs}	Feature	Band Integrated (σ)	Max. Channel (σ)
Sun like	5 pc	10 days	1 ppm all	53.9	4.4
Sun like	5 pc	10 days	10 ppm all	77.0	4.5
Sun like	5 pc	10 days	100 ppm all	101.6	4.8
Sun like	10 pc	50 days	1 ppm all	54.9	5.2
Sun like	10 pc	50 days	10 ppm all	81.1	5.2
Sun like	10 pc	50 days	100 ppm all	107.1	5.4
K6V	5 pc	10 days	1 ppm all	101.7	10.4
K6V	5 pc	10 days	10 ppm all	153.6	10.7
K6V	5 pc	10 days	100 ppm all	206.3	11.2
K6V	10 pc	50 days	1 ppm all	76.6	7.3
K6V	10 pc	50 days	10 ppm all	112.8	7.4
K6V	10 pc	50 days	100 ppm all	144.4	7.3
Trappist like	5 pc	10 days	1 ppm all	138.3	12.7
Trappist like	5 pc	10 days	10 ppm all	187.7	12.0
Trappist like	5 pc	10 days	100 ppm all	207.8	11.3
Trappist like	10 pc	50 days	1 ppm all	27.0	2.6
Trappist like	10 pc	50 days	10 ppm all	38.5	2.4
Trappist like	10 pc	50 days	100 ppm all	46.3	2.1

Note. Results for each technosignature gas individually at 1, 10, and 100 ppm abundance can be found in Appendix B.

are only different by $\sim 20\%$ between cloudy and cloud-free scenarios generated with a 3D global circulation model (GCM; see their Table 4). As we show, artificial greenhouse gases can produce features with substantially larger transit depths than these species at the concentrations we examined (1–100 ppm). In emitted light, we do not include clouds; however, we have previously found that clouds do not substantially impact retrieved abundances of key gases in an Earth-like atmosphere (e.g., Konrad et al. 2023). Assuming clouds have wavelength-independent effects on the emission spectra, they will decrease the emitted light by no more than a factor of 2, and thus the reported band-integrated S/Ns by no more than a factor of $\sqrt{2}$. This would not impact any of our conclusions. Future work

should incorporate these greenhouse gases into 3D GCMs to self-consistently simulate climate and include realistic clouds.

Emitted light spectra are sensitive to the temperature profile of the planet’s atmosphere. As a first-pass assumption, we assumed the modern Earth’s temperature profile. A habitable surface temperature is consistent with the intent of terraforming. However, some greenhouse gases absorb shortwave (UV/visible/NIR) radiation, and can heat the upper atmosphere causing a temperature inversion, as O_3 does in Earth’s atmosphere. Shortwave heating in the upper atmosphere would not only impact the upper atmosphere temperature structure, and thus the emitted light spectrum, but also generate an antigreenhouse effect that will partly act against the greenhouse

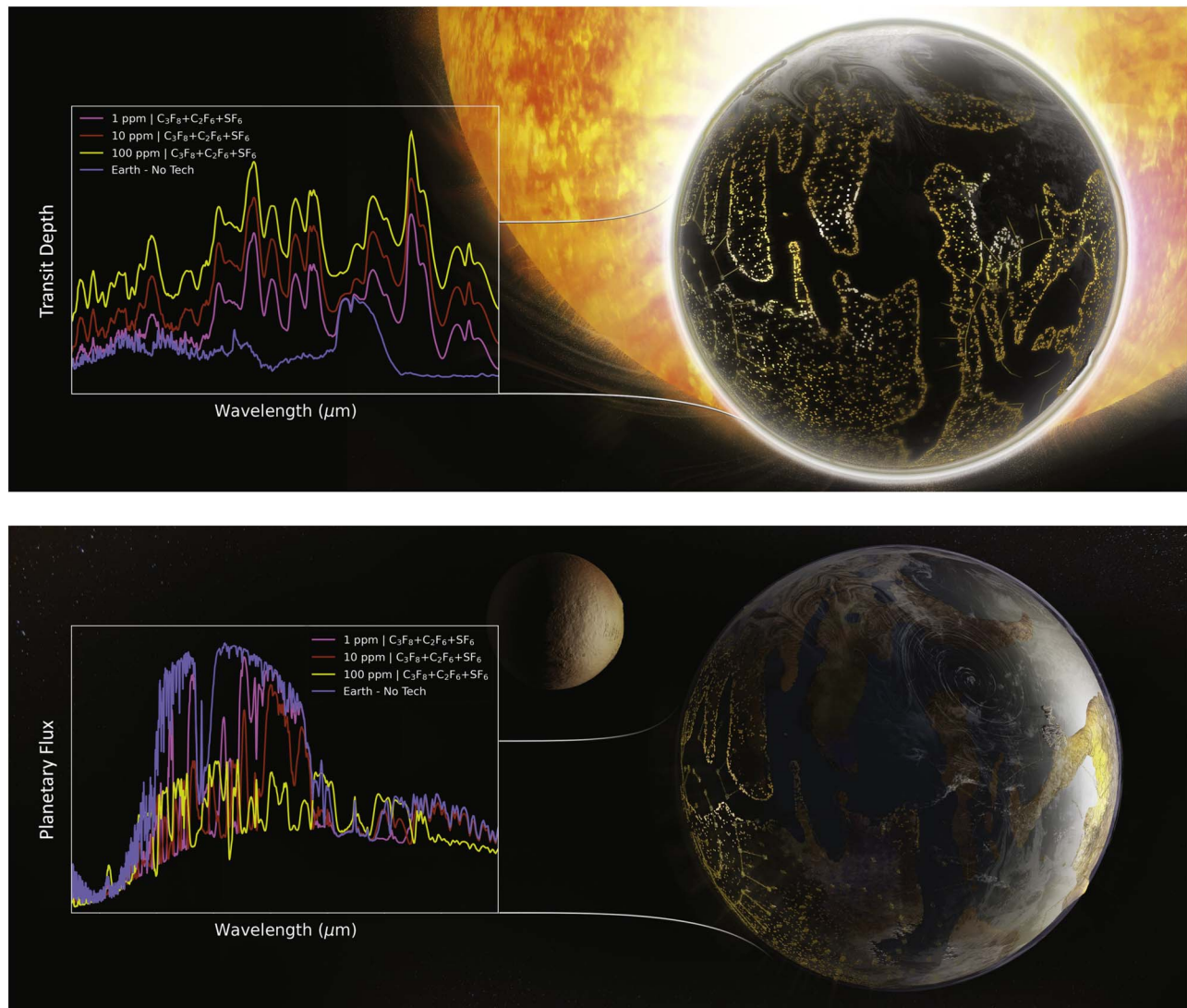


Figure 7. Concept figure illustrating a hypothetical Earth-like inhabited planet terraformed with various combined abundances of artificial greenhouse gases C_3F_8 , C_2F_6 , and SF_6 and its resulting qualitative MIR transmission (top) and emission (bottom) spectra. The figure conveys the anomalously high absorption opacity that may be detected when characterizing an exoplanet whose climate is modified by these artificial gases, which span the key MIR window wavelengths. (Graphic artist: Sohail Wasif, UC Riverside.)

effect of the gas of interest. We do not include this potential effect in our work. Indeed the opacity data for our all five gases examined here (CF_4 , C_2F_6 , C_3F_8 , SF_6 , and NF_3) extend to wavelengths no shorter than $1.5 \mu m$ (Sharpe et al. 2004), which makes such calculations currently impossible. Opacity measurements at the shortest NIR wavelengths ($\sim 1.5\text{--}3 \mu m$) are at or near the detection limit and also have substantial uncertainties. No climate calculations will be truly self-consistent without this shortwave opacity data.

Because we do not have robust opacities at wavelengths relevant to direct imaging of terrestrial planets in reflected light ($\sim 0.2\text{--}2.0 \mu m$), we cannot yet assess the potential detectability of these technosignature gases with the IR/visible/UV surveyor recommended by the 2020 Astronomy & Astrophysics Decadal Survey (National Academies of Sciences, Engineering, & Medicine & others 2023), currently named the HWO. We recommend future opacity measurements for these gases, particularly at visible and NIR wavelengths that are currently unavailable or have high uncertainties. Currently unavailable line-by-line data may be important for assessing

the plausibility of detecting technosignature gases via high-resolution spectroscopy with extremely large telescopes (e.g., Currie et al. 2023; Hardegree-Ullman et al. 2023).

It is also important to mention that our analysis does not assume any noise floor and supposes that the star is perfectly homogeneous. Yet, unocculted starspots (spots on the star's surface not covered by the planet during its transit) cause stellar flux variability. Because starspots are cooler and darker than the surrounding stellar photosphere, they reduce the total stellar flux when present on the visible disk of the star. This variability can be misinterpreted as changes in the planet's transit depth, leading to incorrect interpretations of the planet's atmospheric properties. Specifically, the effect of starspots on observed flux is wavelength dependent, with a more significant impact at shorter wavelengths (Lim et al. 2023) due to the contrast between the cooler spots and the hotter photosphere. This spectral dependence can mimic the wavelength-dependent signals expected from atmospheric features, complicating the differentiation between true atmospheric signals and stellar activity effects. Lim et al. (2023), and references therein,

highlight how the flux variability caused by unocculted starspots imposes an effective noise floor on transmission spectroscopy measurements, and therefore, a lower limit on the detectability of atmospheric features. For planets orbiting active stars like TRAPPIST-1, this noise floor can be particularly problematic because the small size of the star and the planets means that even small changes in stellar flux can significantly impact the measured transit depths. Any atmospheric spectral features with depths lower than 10 ppm, such as SF₆ in the NIR spectrum of Figure 3, are likely to be difficult to detect against this noise floor. The presence of starspots introduces a level of variability that can easily exceed 10 ppm, especially when considering the cumulative effect over multiple transits and the inherent variability in spot coverage over time. Detecting subtle atmospheric features, such as those indicative of certain gases or atmospheric compositions, becomes challenging under these conditions but should improve going to longer wavelengths (see Figure 8 in Appendix A), showcasing the utility of extending planetary characterization into the MIR.

5. Conclusions

We simulated the spectral impact of artificial greenhouse gases on the transmission and emission spectra of Earth-like exoplanets. Specifically, we examined the spectral impact of PFC species CF₄, C₂F₆, and C₃F₈, in addition to SF₆ and NF₃ at concentrations of 1, 10, and 100 ppm. These concentrations are consistent with those required to substantially modify planetary climate. We further calculated the number of transits required to detect 1, 10, and 100 ppm of C₂F₆, C₃F₈, SF₆, and NF₃, or a combination of the first three listed gases on TRAPPIST-1 f with JWST MIR/LRS and NIRSpec. We find that a combination of 1[10](100) ppm each of C₂F₆, C₃F₈, and SF₆ can be detected with an S/N \geq 5 in as few as 25[10](5) transits with MIRI/LRS. Each gas individually can be detected at concentrations of >1 ppm in under 100 transits (except for SF₆ and NF₃ at 1 ppm), and as few as six transits with 100 ppm (C₂F₆). With JWST NIRSpec we find that a combination of 1 [10](100) ppm each of C₂F₆, C₃F₈, and SF₆ can be detected in as few as 80[14](4) transits. Individually, each gas requires at least 36 transits at 100 ppm (C₂F₆). Overall, in transit, C₂F₆ and C₃F₈ both produce stronger spectral signatures than SF₆ and NF₃ at equal concentrations. We analyze the detectability of C₂F₆, C₃F₈, and SF₆ individually and in combination with the MIR direct-imaging LIFE mission concept, and find that all three gases at concentrations \geq 1 ppm produce large spectral features that rival or exceed O₃ at 9.65 μ m and have band-integrated S/N $> 5\sigma$ for all scenarios examined.

We propose that the observation of anomalous MIR (or NIR) absorption in an exoplanetary atmosphere would be consistent with the presence of artificial greenhouse gases in a candidate technosphere. Such anomalous absorption may even be the first indication of a technosphere before any distinguishing features

of individual technosignature gases can be positively confirmed. But such a detection would also raise the possibility that this anomalous absorption is the result of as-yet-unknown planetary processes that do not occur on Earth. Resolving this ambiguity between a technosignature and false positives will ultimately require extended observations to fully characterize the exoplanetary environment.

Future work should examine climatically self-consistent scenarios, though we note that additional opacity information is likely required, especially at NIR and visible wavelengths. Short-wavelength opacity data of technosignature gases would also be required to assess their detectability with an IR/visible/UV surveyor mission such as HWO. We conclude that artificial greenhouse gases are viable technosignatures that can be detected during otherwise routine planetary characterization operations at infrared wavelengths. Both positive or negative results would meaningfully inform the search for life elsewhere.

Acknowledgments

This study resulted in part from the TechnoClimes workshop (2020 August 3–7, <http://technoclimes.org>), which was supported by the NASA Exobiology program under award 80NSSC20K1109. We acknowledge additional support from the NASA Interdisciplinary Consortium for Astrobiology Research (ICAR) Program under grant Nos. 80NSSC21K0905, 80NSSC23K1399, and 80NSSC21K0594. J.H.M. and R.K.K. also acknowledge support from the NASA Exobiology program under grant 80NSSC22K1009. The statements in this study do not necessarily reflect the views of NASA or any other funding agency or institution. D.A.'s work has been carried out within the framework of the National Centre of Competence in Research PlanetS supported by the Swiss National Science Foundation under grants 51NF40_182901 and 51NF40_205606. We thank UCR graphic artist Sohail Wasif for his assistance in creating the concept figure shown in the Discussion section. We thank Kevin Stevenson for helpful input regarding the noise modeling. We are also grateful to the anonymous referee for comments that allowed us to improve the paper.

Software: SMART (Meadows & Crisp 1996; Crisp 1997), PSG (Villanueva et al. 2018, 2022), LIFESIM (Dannert et al. 2022), Matplotlib (Hunter 2007), and NumPy (Harris et al. 2020).

Appendix A

Transit Depth Uncertainty for NIRSpec Prism and MIRI LRS

Figure 8 shows the transit depth uncertainty (parts per million) corresponding to the simulations shown in Figures 2 and 3.

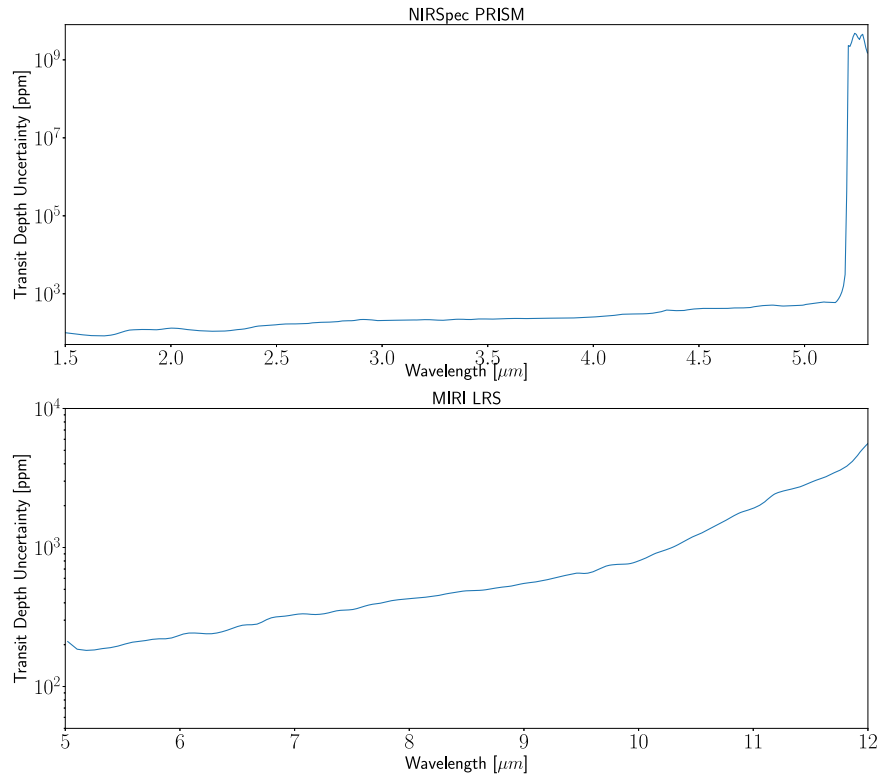


Figure 8. Top: transit depth uncertainty (in units of ppm) for the NIRSpec prism (restricted in the wavelength range where technosignature gas absorption are located). Bottom: transit depth uncertainty (in units of ppm) for MIRI LRS.

Appendix B Additional Tables for the LIFE Simulations

Table 6 provides the band-integrated and maximum in channel S/Ns for individual technosignature gases in an Earth-

like atmosphere calculated using LIFESIM as described in Sections 2.3 and 3.3.1. The corresponding emission spectra are calculated with SMART as described in Section 2.2 and shown in Section 3.3.

Table 6
Detectability of Individual Technosignature Gases with LIFE Calculated with LIFESIM

Host Star	Distance	T_{obs}	Feature	Band-int. (σ)	Max. Channel (σ)
SF₆					
Sun like	5 pc	10 days	1 ppm SF ₆	25.3	4.4
Sun like	5 pc	10 days	10 ppm SF ₆	41.7	4.5
Sun like	5 pc	10 days	100 ppm SF ₆	63.6	4.6
Sun like	10 pc	50 days	1 ppm SF ₆	27.1	5.2
Sun like	10 pc	50 days	10 ppm SF ₆	46.2	5.2
Sun like	10 pc	50 days	100 ppm SF ₆	69.5	5.5
K6V	5 pc	10 days	1 ppm SF ₆	52.9	10.4
K6V	5 pc	10 days	10 ppm SF ₆	91.0	10.5
K6V	5 pc	10 days	100 ppm SF ₆	135.2	11.3
K6V	10 pc	50 days	1 ppm SF ₆	36.1	7.3
K6V	10 pc	50 days	10 ppm SF ₆	63.4	7.4
K6V	10 pc	50 days	100 ppm SF ₆	95.3	7.3
Trappist like	5 pc	10 days	1 ppm SF ₆	42.5	9.0
Trappist like	5 pc	10 days	10 ppm SF ₆	83.1	10.3
Trappist like	5 pc	10 days	100 ppm SF ₆	134.9	9.9
Trappist like	10 pc	50 days	1 ppm SF ₆	7.4	1.5
Trappist like	10 pc	50 days	10 ppm SF ₆	15.0	1.8
Trappist like	10 pc	50 days	100 ppm SF ₆	25.6	1.9
C₂F₆					
Sun like	5 pc	10 days	1 ppm C ₂ F ₆	14.3	3.8
Sun like	5 pc	10 days	10 ppm C ₂ F ₆	28.3	3.6

Table 6
(Continued)

Host Star	Distance	T_{obs}	Feature	Band-int. (σ)	Max. Channel (σ)
Sun like	5 pc	10 days	100 ppm C_2F_6	56.3	3.8
Sun like	10 pc	50 days	1 ppm C_2F_6	13.6	3.5
Sun like	10 pc	50 days	10 ppm C_2F_6	27.1	3.3
Sun like	10 pc	50 days	100 ppm C_2F_6	55.1	3.6
K6V	5 pc	10 days	1 ppm C_2F_6	23.4	6.2
K6V	5 pc	10 days	10 ppm C_2F_6	47.1	5.6
K6V	5 pc	10 days	100 ppm C_2F_6	100.0	7.0
K6V	10 pc	50 days	1 ppm C_2F_6	19.9	5.3
K6V	10 pc	50 days	10 ppm C_2F_6	39.3	5.0
K6V	10 pc	50 days	100 ppm C_2F_6	76.3	5.4
Trappist like	5 pc	10 days	1 ppm C_2F_6	48.6	12.2
Trappist like	5 pc	10 days	10 ppm C_2F_6	94.4	12.3
Trappist like	5 pc	10 days	100 ppm C_2F_6	148.2	12.2
Trappist like	10 pc	50 days	1 ppm C_2F_6	10.0	2.3
Trappist like	10 pc	50 days	10 ppm C_2F_6	20.7	2.5
Trappist like	10 pc	50 days	100 ppm C_2F_6	34.1	2.4
C_3F_8					
Sun like	5 pc	10 days	1 ppm C_3F_8	23.5	3.2
Sun like	5 pc	10 days	10 ppm C_3F_8	44.2	4.0
Sun like	5 pc	10 days	100 ppm C_3F_8	77.9	4.8
Sun like	10 pc	50 days	1 ppm C_3F_8	23.3	3.1
Sun like	10 pc	50 days	10 ppm C_3F_8	45.0	4.4
Sun like	10 pc	50 days	100 ppm C_3F_8	82.4	5.4
K6V	5 pc	10 days	1 ppm C_3F_8	40.9	6.0
K6V	5 pc	10 days	10 ppm C_3F_8	82.0	8.5
K6V	5 pc	10 days	100 ppm C_3F_8	157.0	11.0
K6V	10 pc	50 days	1 ppm C_3F_8	33.8	4.6
K6V	10 pc	50 days	10 ppm C_3F_8	63.9	6.3
K6V	10 pc	50 days	100 ppm C_3F_8	113.3	6.9
Trappist like	5 pc	10 days	1 ppm C_3F_8	79.8	12.6
Trappist like	5 pc	10 days	10 ppm C_3F_8	129.4	11.9
Trappist like	5 pc	10 days	100 ppm C_3F_8	180.8	12.5
Trappist like	10 pc	50 days	1 ppm C_3F_8	16.3	2.6
Trappist like	10 pc	50 days	10 ppm C_3F_8	27.0	2.5
Trappist like	10 pc	50 days	100 ppm C_3F_8	40.5	2.4
NF_3					
Sun like	5 pc	10 days	1 ppm NF_3	24.6	4.6
Sun like	5 pc	10 days	10 ppm NF_3	43.1	4.5
Sun like	5 pc	10 days	100 ppm NF_3	62.8	4.9
Sun like	10 pc	50 days	1 ppm NF_3	28.5	5.5
Sun like	10 pc	50 days	10 ppm NF_3	48.5	5.4
Sun like	10 pc	50 days	100 ppm NF_3	68.4	5.8
K6V	5 pc	10 days	1 ppm NF_3	57.2	11.2
K6V	5 pc	10 days	10 ppm NF_3	95.9	11.0
K6V	5 pc	10 days	100 ppm NF_3	133.1	12.0
K6V	10 pc	50 days	1 ppm NF_3	39.7	7.5
K6V	10 pc	50 days	10 ppm NF_3	68.1	7.2
K6V	10 pc	50 days	100 ppm NF_3	95.8	7.7
Trappist like	5 pc	10 days	1 ppm NF_3	49.2	8.3
Trappist like	5 pc	10 days	10 ppm NF_3	92.7	9.2
Trappist like	5 pc	10 days	100 ppm NF_3	142.0	11.6
Trappist like	10 pc	50 days	1 ppm NF_3	8.6	1.4
Trappist like	10 pc	50 days	10 ppm NF_3	17.4	1.6
Trappist like	10 pc	50 days	100 ppm NF_3	28.7	2.3
CF_4					
Sun like	5 pc	10 days	1 ppm CF_4	4.2	1.3
Sun like	5 pc	10 days	10 ppm CF_4	11.3	2.4
Sun like	5 pc	10 days	100 ppm CF_4	25.2	3.0
Sun like	10 pc	50 days	1 ppm CF_4	3.9	1.3
Sun like	10 pc	50 days	10 ppm CF_4	10.4	2.1
Sun like	10 pc	50 days	100 ppm CF_4	24.1	2.8

Table 6
(Continued)

Host Star	Distance	T_{obs}	Feature	Band-int. (σ)	Max. Channel (σ)
K6V	5 pc	10 days	1 ppm CF ₄	6.4	1.9
K6V	5 pc	10 days	10 ppm CF ₄	18.3	3.9
K6V	5 pc	10 days	100 ppm CF ₄	42.8	5.2
K6V	10 pc	50 days	1 ppm CF ₄	5.4	1.9
K6V	10 pc	50 days	10 ppm CF ₄	13.5	2.3
K6V	10 pc	50 days	100 ppm CF ₄	32.2	4.3
Trappist like	5 pc	10 days	1 ppm CF ₄	15.4	7.0
Trappist like	5 pc	10 days	10 ppm CF ₄	26.9	6.8
Trappist like	5 pc	10 days	100 ppm CF ₄	63.6	9.0
Trappist like	10 pc	50 days	1 ppm CF ₄	3.4	1.5
Trappist like	10 pc	50 days	10 ppm CF ₄	6.1	1.4
Trappist like	10 pc	50 days	100 ppm CF ₄	14.8	1.9

Note. The corresponding data for 1, 10, and 100 ppm combinations of C₂F₆ + C₃F₈ + SF₆ can be found in Table 5.


ORCID iDs

Edward W. Schwieterman  <https://orcid.org/0000-0002-2949-2163>

Thomas J. Fauchez  <https://orcid.org/0000-0002-5967-9631>

Jacob Haqq-Misra  <https://orcid.org/0000-0003-4346-2611>

Ravi K. Kopparapu  <https://orcid.org/0000-0002-5893-2471>

Daniel Angerhausen  <https://orcid.org/0000-0001-6138-8633>

Daria Pidhorodetska  <https://orcid.org/0000-0001-9771-7953>

Michaela Leung  <https://orcid.org/0000-0003-1906-5093>

Evan L. Sneed  <https://orcid.org/0000-0001-5290-1001>

Elsa Ducrot  <https://orcid.org/0000-0002-7008-6888>

References

- Alei, E., Konrad, B. S., Angerhausen, D., et al. 2022, *A&A*, 665, A106
- Angerhausen, D., Ottiger, M., Dannert, F., et al. 2023, *AsBio*, 23, 183
- Angerhausen, D., Pidhorodetska, D., Leung, M., et al. 2024, *AJ*, 167, 128
- Arney, G., Meadows, V., Crisp, D., et al. 2014, *JGRE*, 119, 1860
- Arnold, T., Harth, C. M., Mühle, J., et al. 2013, *PNAS*, 110, 2029
- Bagnasco, G., Kolm, M., Ferrut, P., et al. 2007, *Proc. SPIE*, 6692, 66920M
- Beatty, T. G. 2022, *MNRAS*, 513, 2652
- Berger, A. 1988, *RvGeo*, 26, 624
- Bowyer, S., Werthimer, D., & Lindsay, V. 1988, in *Bioastronomy—The Next Steps*, ed. G. Marx (Dordrecht: Springer), 363
- Charnay, B., Meadows, V., Misra, A., Leconte, J., & Arney, G. 2015, *ApJL*, 813, L1
- Cocconi, G., & Morrison, P. 1959, *Natur*, 184, 844
- Cooke, G. J., Marsh, D. R., Walsh, C., & Youngblood, A. 2023, *ApJ*, 959, 45
- Crisp, D. 1997, *GeoRL*, 24, 571
- Currie, M. H., Meadows, V. S., & Rasmussen, K. C. 2023, *PSJ*, 4, 83
- Czech, D., Isaacson, H., Pearce, L., et al. 2021, *PASP*, 133, 064502
- Carrión-González, Ó., Kammerer, J., Angerhausen, D., et al. 2023, *A&A*, 678, A96
- Dannert, F. A., Ottiger, M., Quanz, S. P., et al. 2022, *A&A*, 664, A22
- DeBoer, D. R. 2006, *AcAau*, 59, 1153
- Dicaire, I., Forget, F., Millour, E., et al. 2013, in 64th International Astronautical Congress, IAC-13 (Beijing: IAF) D3, 3.10x19180
- Dyson, F. J. 1960, *Sci*, 131, 1667
- Elowitz, M. 2022, AAS Meeting, 240, 402.07
- Elsayed, N. 1994, *Toxicology*, 89, 161
- Ertel, S., Defrère, D., Hinz, P., et al. 2020, *AJ*, 159, 177
- Fahey, D., Newman, P. A., Pyle, J. A., et al. 2018, Scientific Assessment of Ozone Depletion: 2018, Global Ozone Research and Monitoring Project 58, World Meteorological Organization, <https://hal.science/hal-02344136/>
- Fauchez, T. J., Turbet, M., Villanueva, G. L., et al. 2019, *ApJ*, 887, 194
- Fauchez, T. J., Villanueva, G. L., Schwieterman, E. W., et al. 2020, *NatAs*, 4, 372
- Fauchez, T. J., Villanueva, G. L., Sergeev, D. E., et al. 2022, *PSJ*, 3, 213
- Frank, A., Kleidon, A., & Alberti, M. 2017, *Anthropocene*, 19, 13
- Gaudi, B. S., Seager, S., Mennesson, B., et al. 2020, arXiv:2001.06683
- Gordon, I. E., Rothman, L. S., Hargreaves, R. J., et al. 2022, *JQSRT*, 277, 107949
- Graham, J. M. 2004, *AsBio*, 4, 168
- Haqq-Misra, J. 2014, *JAMES*, 6, 950
- Haqq-Misra, J., Kopparapu, R., Fauchez, T. J., et al. 2022a, *PSJ*, 3, 60
- Haqq-Misra, J., Kopparapu, R. K., & Schwieterman, E. 2020, *AsBio*, 20, 572
- Haqq-Misra, J., Schwieterman, E. W., Socas-Navarro, H., et al. 2022b, *AcAau*, 198, 194
- Hardegreve-Ullman, K. K., Apai, D., Bergsten, G. J., Pascucci, I., & López-Morales, M. 2023, *AJ*, 165, 267
- Harnisch, J., & Eisenhauer, A. 1998, *GeoRL*, 25, 2401
- Harris, C. R., Millman, K. J., Van Der Walt, S. J., et al. 2020, *Natur*, 585, 357
- Howard, A., Horowitz, P., Mead, C., et al. 2007, *AcAau*, 61, 78
- Hu, L., Montzka, S. A., Lehman, S. J., et al. 2017, *GeoRL*, 44, 8075
- Hunter, J. D. 2007, *CSE*, 9, 90
- Illuzzi, F., & Thewissen, H. 2010, *JIES*, 7, 201
- Jakosky, B. M., & Edwards, C. S. 2018, *NatAs*, 2, 634
- Kaltenegger, L. 2017, *ARA&A*, 55, 433
- Kammerer, J., & Quanz, S. P. 2018, *A&A*, 609, A4
- Kammerer, J., Quanz, S. P., Dannert, F., & LIFE Collaboration 2022, *A&A*, 668, A52
- Kochanov, R. V., Gordon, I. E., Rothman, L. S., et al. 2019, *JQSRT*, 230, 172
- Konrad, B. S., Alei, E., Quanz, S. P., et al. 2022, *A&A*, 664, A23
- Konrad, B. S., Alei, E., Quanz, S. P., et al. 2023, *A&A*, 673, A94
- Kopparapu, R., Arney, G., Haqq-Misra, J., Lustig-Yaeger, J., & Villanueva, G. 2021, *ApJ*, 908, 164
- Kopparapu, R. K., Ramirez, R., Kasting, J. F., et al. 2013, *ApJ*, 765, 131
- Kovács, T., Feng, W., Totterdill, A., et al. 2017, *ACP*, 17, 883
- Krissansen-Totton, J., Garland, R., Irwin, P., & Catling, D. C. 2018a, *AJ*, 156, 114
- Krissansen-Totton, J., Olson, S., & Catling, D. C. 2018b, *SciA*, 4, eaao5747
- Lan, X., Thoning, K., & Dlugokencky, E. 2023, Trends in globally-averaged CH₄, N₂O, and SF₆ determined from NOAA Global Monitoring Laboratory measurements, v2023-12, doi:10.15138/P8XG-AA10
- Leung, M., Schwieterman, E. W., Parenteau, M. N., & Fauchez, T. J. 2022, *ApJ*, 938, 6
- Lim, O., Benneke, B., Doyon, R., et al. 2023, *ApJL*, 955, L22
- Lin, H. W., Abad, G. G., & Loeb, A. 2014, *ApJL*, 792, L7
- Lingam, M., & Loeb, A. 2017, *MNRAS: Letters*, 470, L82
- Lingam, M., & Loeb, A. 2019, *AsBio*, 19, 28
- Lodders, K., & Fegley, B., Jr. 2015, *Chemistry of the Solar System* (Cambridge: Royal Society of Chemistry)
- Lustig-Yaeger, J., Fu, G., May, E. M., et al. 2023a, *NatAs*, 7, 1317
- Lustig-Yaeger, J., Meadows, V. S., Crisp, D., Line, M. R., & Robinson, T. D. 2023b, *PSJ*, 4, 170
- Lustig-Yaeger, J., Meadows, V. S., & Lincowski, A. P. 2019, *AJ*, 158, 27
- Luther, F. M., Ellingson, R. G., Fouquart, Y., et al. 1988, *BAMS*, 69, 40
- LUVOIR-Team 2019, arXiv:1912.06219
- Macdonald, E. J. R., & Cowan, N. B. 2019, *MNRAS*, 489, 196

- Maione, M., Giostra, U., Arduini, J., et al. 2013, *ScTEen*, **445**, 155
- Marinova, M. M., McKay, C. P., & Hashimoto, H. 2005, *JGRE*, **110**, E03002
- Meadows, V. S., & Crisp, D. 1996, *JGR*, **101**, 4595
- Meadows, V. S., Lincowski, A. P., & Lustig-Yaeger, J. 2023, *PSJ*, **4**, 192
- Meadows, V. S., Reinhard, C. T., Arney, G. N., et al. 2018, *AsBio*, **18**, 630
- Mikal-Evans, T. 2021, *MNRAS*, **510**, 980
- Mühle, J., Ganesan, A. L., Miller, B. R., et al. 2010, *ACP*, **10**, 5145
- Myhre, G., Shindell, D., Bréon, F.-M., et al. 2013, in *Climate Change 2013—The Physical Science Basis*, ed. Intergovernmental Panel on Climate Change (Cambridge: Cambridge Univ. Press), 659
- National Academies of Sciences, Engineering, and Medicine and others 2018, *Exoplanet Science Strategy* (Washington, DC: The National Academies Press)
- National Academies of Sciences, Engineering, and Medicine and others 2019, *Astrobiology Strategy for the Search for Life in the Universe* (Washington, DC: The National Academies Press)
- National Academies of Sciences, Engineering, and Medicine and others 2023, *Pathways to Discovery in Astronomy and Astrophysics for the 2020s* (Washington, DC: The National Academies Press)
- NASA Technosignatures Workshop Participants 2018, arXiv:1812.08681
- Olson, S. L., Schwieterman, E. W., Reinhard, C. T., & Lyons, T. W. 2018, in *Handbook of Exoplanets*, ed. H. Deeg & J. Belmont (Cham: Springer), 189
- Ostberg, C., Kane, S. R., Lincowski, A. P., & Dalba, P. A. 2023, *AJ*, **166**, 213
- Pałka, P., Olszewski, R., & Wendland, A. 2022, *Energies*, **15**, 4957
- Pidhorodetska, D., Fauchez, T. J., Villanueva, G. L., Domagal-Goldman, S. D., & Kopparapu, R. K. 2020, *ApJL*, **898**, L33
- Prinn, R., Weiss, R. F., Arduini, J., et al. 2018a, *History of Chemically and Radiatively Important Atmospheric Gases from the Advanced Global Atmospheric Gases Experiment (AGAGE)*, CDIAC, ORNL, doi:10.3334/CDIAC/ATG.DB1001
- Prinn, R. G., Weiss, R. F., Arduini, J., et al. 2018b, *ESSD*, **10**, 985
- Quanz, S. P., Ottiger, M., Fontanet, E., et al. 2022, *A&A*, **664**, A21
- Ramirez, R. M. 2020, *NatSR*, **10**, 7432
- Ray, E. A., Moore, F. L., Elkins, J. W., et al. 2017, *JGRD*, **122**, 4626
- Robinson, T. D., Ennico, K., Meadows, V. S., et al. 2014a, *ApJ*, **787**, 171
- Robinson, T. D., Maltagliati, L., Marley, M. S., & Fortney, J. J. 2014b, *PNAS*, **111**, 9042
- Schwieterman, E. W., Kiang, N. Y., Parenteau, M. N., et al. 2018, *AsBio*, **18**, 663
- Schwieterman, E. W., Olson, S. L., Pidhorodetska, D., et al. 2022, *ApJ*, **937**, 109
- Schwieterman, E. W., Reinhard, C. T., Olson, S. L., Harman, C. E., & Lyons, T. W. 2019, *ApJ*, **878**, 19
- Seager, S., Petkowski, J. J., Huang, J., et al. 2023, *NatSR*, **13**, 13576
- Seager, S., Schrenk, M., & Bains, W. 2012, *AsBio*, **12**, 61
- Sharpe, S. W., Johnson, T. J., Sams, R. L., et al. 2004, *ApSpe*, **58**, 1452
- Sheikh, S. Z. 2020, *IJAsB*, **19**, 237
- Shields, A. L., Barnes, R., Agol, E., et al. 2016, *AsBio*, **16**, 443
- Shkadov, L. M. 1988, *SoSyR*, **22**, 210
- Solomon, S. 1999, *RvGeo*, **37**, 275
- Stone, R., Wright, S., Drake, F., et al. 2005, *AsBio*, **5**, 604
- Suissa, G., Mandell, A. M., Wolf, E. T., et al. 2020, *ApJ*, **891**, 58
- Sullivan, W. T., III, Werthimer, D., Bowyer, S., et al. 1997, in *IAU Colloq. 161: Astronomical and Biochemical Origins and the Search for Life in the Universe*, ed. C. B. Cosmovici, S. Bowyer, & D. Werthimer (Bologna: Editrice Compositori), 729
- Tarter, J. 2001, *ARA&A*, **39**, 511
- Tarter, J. C. 2007, *Proc. IAU 14, Highlights of Astronomy* (Cambridge: Cambridge Univ. Press), 14
- Tinetti, G., Meadows, V. S., Crisp, D., et al. 2005, *AsBio*, **5**, 461
- Totterdill, A., Kovács, T., Feng, W., et al. 2016, *ACP*, **16**, 11451
- Tremblay, C. D., Varghese, S. S., Hickish, J., et al. 2024, *AJ*, **167**, 35
- Trudinger, C. M., Fraser, P. J., Etheridge, D. M., et al. 2016, *ACP*, **16**, 11733
- UNFCCC COP 19 2013, *Report on COP 19 (FCCC/CP/2013/10/Add.3)*, Tech. Rep., <http://unfccc.int/resource/docs/2013/cop19/eng/10a03.pdf>
- Vides, C. L., Macintosh, B., Binder, B. A., et al. 2019, *AJ*, **158**, 207
- Villanueva, G. L., Liuzzi, G., Faggi, S., et al. 2022, *Fundamentals of the Planetary Spectrum Generator* (Greenbelt, MD: NASA Goddard Space Flight Center)
- Villanueva, G. L., Smith, M. D., Protopapa, S., Faggi, S., & Mandell, A. M. 2018, *JQSRT*, **217**, 86
- Worden, S. P., Drew, J., Siemion, A., et al. 2017, *AcAau*, **139**, 98
- Wright, G. S., Rieke, G. H., Colina, L., et al. 2004, *Proc. SPIE*, **5487**, 653
- Wright, J. T. 2020, *SerAJ*, **200**, 1
- Wright, J. T., Haqq-Misra, J., Frank, A., et al. 2022, *ApJL*, **927**, L30